Engineering Structures 168 (2018) 142–162

Contents lists available at ScienceDirect

Engineering Structures

journal homepage: www.elsevier.com/locate/engstruct

Seismic assessment and loss estimation of existing school buildings in Italy

Gerard J. O'Reilly[a,*], Daniele Perrone[a], Matthew Fox[b], Ricardo Monteiro[a], Andre Filiatrault[a,c]

[a] University School for Advanced Studies IUSS Pavia, Palazzo del Broletto, Piazza della Vittoria 15, Pavia 27100, Italy
[b] Beca Limited, Christchurch 8011, New Zealand
[c] Department of Civil, Structural, and Environmental Engineering, State University of New York at Buffalo, NY 14260, USA

ARTICLE INFO

Keywords:
Seismic assessment
Loss estimation
Vulnerability
School buildings
Collapse

ABSTRACT

Extensive damage to school buildings has been observed during past earthquakes in Italy and there is a need to better understand their potential vulnerability. As part of a national project to assess seismic risk in Italian schools, a database was compiled in terms of characteristics such as school location and construction typology. This paper examines a number of these buildings considered to be a representative sample of the Italian school building population. To quantify their seismic vulnerability, the induced damage with respect to increased shaking intensity need to be quantified. This characterisation of the building vulnerability, in combination with the seismic hazard, allows more informed, risk-based decisions to be made using performance metrics such as expected annual loss (EAL). This article outlines a case study application quantifying the EAL and collapse safety for three school buildings representative of the Italian school building stock. Detailed numerical models were developed using information collected during in-situ inspections in order to accurately represent the dynamic response of the school structures. To estimate economic losses, a structural and non-structural element inventory was compiled using in-situ survey information. This case study application is conducted in a systematic fashion to clearly illustrate the various details required to implement more advanced seismic assessment studies. Finally, a comparison is made with the seismic classification guidelines recently introduced in Italy to provide further insight into how these can be used to identify existing buildings vulnerable to excessive damage and potential collapse during earthquakes.

1. Introduction

The seismic vulnerability of existing school buildings in Italy has received much attention following the 2002 Molise earthquake in Southern Italy, which resulted in the collapse of the Iovene primary school in San Giuliano killing 27 students and one teacher. To address this issue, the European Centre for Training and Research in Earthquake Engineering (EUCENTRE) initiated a research project entitled '*Progetto Scuole*', with the main objective of seismically assessing a number of school buildings throughout Italy that can be considered representative of the existing school building stock. Survey information [1] showed that the majority of reinforced concrete (RC) frame school buildings were constructed prior to the 1970s with little to no consideration of modern seismic design principles. These RC buildings were typically designed for gravity loads only and involved using allowable stress and other such design provisions specified in Regio Decreto 2229/1939 [2] along with other common construction conventions prior to the introduction of seismic design provisions [3]. A common feature of these gravity load-only designs identified in O'Reilly et al. [4] is the complete lack of capacity design considerations in the beam and column members of RC frames. The columns were sized principally for axial loading and the beam members were designed by considering the hogging and sagging moments of a continuously loaded multi-support beam. This approach was quite common during the construction boom that followed World War II across southern Europe and gave rise to many RC structures vulnerable to undesirable seismic response, as highlighted during past earthquakes [5–8]. Unreinforced masonry buildings (URM) were also seen to represent a significant portion of the building stock in Italy, with many being historical and/or old masonry buildings known to be seismically vulnerable [9]. For example, field observations from the Emilia Romagna earthquake in 2012 [10] underlined this through numerous partial collapses observed in historical masonry buildings. Furthermore, the presence of large thin unsupported clear lengths of masonry can result in the wall ejection mechanism, a type of behaviour observed in scholastic structures in L'Aquila [11], for example. The response of URM buildings not vulnerable to this kind of local failure mode is generally governed by in-plane behaviour of the walls, causing piers and spandrel damage. Spandrel shear and flexural failure has been

* Corresponding author.
E-mail address: gerard.oreilly@iusspavia.it (G.J. O'Reilly).

https://doi.org/10.1016/j.engstruct.2018.04.056
Received 3 August 2017; Received in revised form 12 February 2018; Accepted 16 April 2018

commonly observed in the past [10] and is mainly related to the quality of the supporting lintels [12]. In addition, another common damage mechanism is pier member damage [10], accompanied by shear diagonal cracking similar to that observed in spandrels. In some cases, the lack of maintenance contributed to increase the seismic vulnerability of existing masonry buildings, such as the degradation of timber, which can reduce the efficiency of the floor system to provide rigid diaphragm action when transferring inertial forces to the lateral load resisting system. Precast Concrete (PC) structures have also been used extensively in Italy, most commonly for industrial buildings. The seismic vulnerability of this structural typology has been observed in numerous past earthquakes, in particular the 2012 Emilia earthquakes, which resulted in a significant number of casualties and economic losses. From post-earthquake reconnaissance, Magliulo et al. [13] reported that the observed damage in PC buildings was mainly related to either loss of support of horizontal elements or the collapse of cladding panels, with both cases being the result of poor connection detailing. The poor seismic detailing that is typical in these buildings is likely to be a result of the first specific precast regulations only being published in 1987 in Italy.

A significant portion of the total losses in recent earthquakes worldwide has been attributed to damage to non-structural elements, which occurs at low levels of ground shaking and can significantly affect the post-earthquake functionality of buildings. Typical damage is related to ceiling systems, piping systems, infill walls and building contents. An example of extensive damage to non-structural elements was reported by Miranda et al. [14] following the 2010 Maule Earthquake in Chile; the Santiago International Airport was closed for several days due to significant damage to piping and ceiling systems, while four hospitals completely lost their functionality and over ten lost 75% of their functionality due to damage to fire sprinklers. Braga et al. [15] reported extensive in-plane and out-of-plane damage to masonry infills in RC buildings during the 2009 L'Aquila Earthquake in Italy. Likewise following the 2012 Emilia Earthquake, where storage rack systems in industrial facilities were the most affected components [16]. Calvi et al. [17] conducted an exhaustive review of typical non-structural damage observed in school buildings after major seismic events around the world and highlighted that ceiling systems, partitions, lighting systems and bookshelves are generally the most vulnerable elements. The main reasons identified were the lack of proper anchorage of the various elements and, in many cases, the absence of clear seismic design methodologies and prescriptions to implement.

In terms of assessing the performance of buildings and their structural and non-structural elements, one of the most comprehensive PBEE methodologies was initially conceived by Cornell and Krawinkler [18] and then adopted by the Pacific Earthquake Engineering Research Center (PEER). This PEER-PBEE framework includes a number of stages, illustrated in Fig. 1.1, with hazard, structural, damage and loss analysis being conducted to provide information for a final consequence analysis of performance measures referred to as decision variables (DV), such as the expected losses and also collapse safety. The practical implementation of each individual step of this framework has also been described in detail by Gunay and Mosalam [19].

If one considers the expected monetary losses due to the repairs required at each intensity measure (IM) level, the expected annual loss (EAL) of a building for a given site location can be computed by integrating the expected direct economic losses expressed as a function of IM over the site hazard curve obtained from PSHA, as indicated in Eq. (2):

$$EAL = \int E[L_T \,|IM] \left| \frac{d\lambda}{dIM} \right| dIM \tag{2}$$

where $E[L_T|IM]$ represents the total expected direct economic losses for a given definition of IM and site D, as described above.

In 2017, the Italian Ministry of Infrastructure and Transport issued Decreto Ministeriale 58/2017 [20] outlining a framework with which to classify the seismic risk of buildings. The building's seismic performance is described in terms of EAL and structural collapse capacity, which are employed to give an overall rating on a letter-based scale from A+ to G, similar to the appliances energy consumption scale used in Europe [21]. This framework is integrated with the existing Italian code [22] to provide practitioners with a more simplified method and metric to assess the overall seismic performance of buildings via retrofitting.

This paper examines the seismic loss assessment of buildings by characterising and comparing the vulnerability of existing school buildings in Italy using the PEER-PBEE detailed framework outlined in the FEMA P58 document [23]. This is implemented in a systematic fashion, whereby a representative sample of three buildings from the entire existing school building stock was identified and examined in detail, involving the collection of data regarding both the structural configuration and the non-structural element inventory. Detailed numerical models were constructed for each school building to characterise the seismic response to increasing seismic intensity, which was then used in conjunction with the inventoried list of damageable components identified during in-situ inspections of each school building to conduct a detailed loss estimation study for each of them. This was performed for three different building construction typologies, namely RC frames with masonry infill, URM buildings and PC frames, typically found throughout Italy. The results of this study allow for the vulnerability of each school building typology to be characterised and compared. Furthermore, it is hoped that the detailed case study application presented herein will encourage more practitioners to use available comprehensive methods to assess seismic vulnerability of existing buildings. Lastly, comparison of the detailed analysis conducted here with the recent Italian guidelines to classify seismic risk is discussed in order to illustrate some differences and potential future improvements to the guidelines.

2. Case study school buildings

A number of school buildings comprising different structural typologies were selected for this study. Available information on over 49,000 Italian schools [1] was examined to determine the prevalent

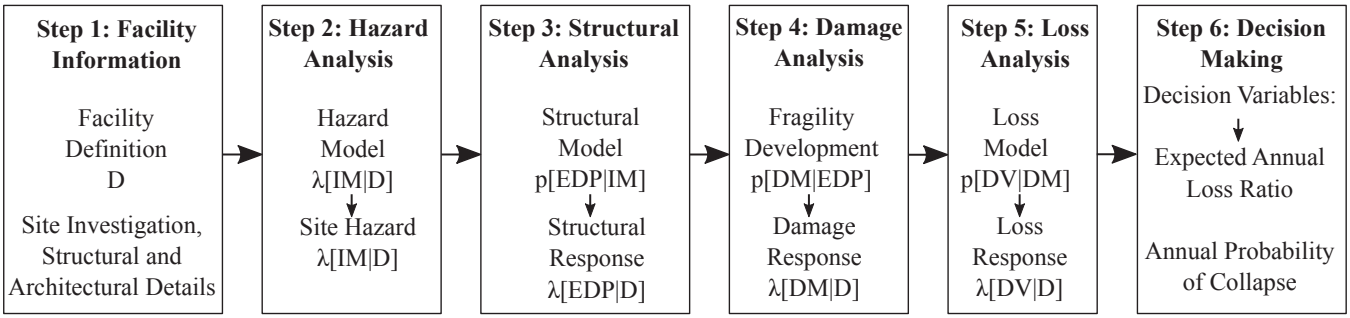

Fig. 1.1. Illustration of the four stages of the PEER-PBEE framework [18].

Table 2.1
General information for case study school buildings.

Typology	Label	No. of storeys	Construction period
Reinforced concrete frame with masonry infill	RC	3	1960s
Unreinforced masonry	URM	2	1900s
Precast RC frame	PC	2	1980s

characteristics of the existing building stock so a representative sample could be established and further examined. This information showed that the majority of scholastic buildings have three or fewer storeys and commonly consisted of RC frames with masonry infills or URM; where the older the building is, the more likely it was constructed with URM. More recent PC buildings represent a smaller portion of the existing school building stock. Furthermore, approximately 67% of the existing school buildings in Italy have been constructed before 1975, which precedes the introduction of modern seismic design provisions in the country. Considering the above points regarding age and construction typology, Table 2.1 lists the three school buildings chosen for this study. The construction typology, number of storeys and construction periods of these three case study buildings were found to correspond well with the overall characteristics of the existing scholastic building stock as a whole. It is noted also that for each of these three buildings, no modern seismic design provisions were implemented in their design.

3. Assessment of Italian school buildings

For each of the school buildings outlined in Section 2, a complete loss estimation study was carried out using the PEER-PBEE methodology described in Section 1. While the assessment procedure described herein was largely based on that prescribed in the FEMA P58 guidelines [23], this case study application aimed to provide a more practice-orientated application of the methodology. As such, a breakdown of the method into a more systematic approach that practitioners can then implement in future studies was carried out and is illustrated in Fig. 3.1. The more conceptual layout of the procedure is used, offering a useful and succinct description of the methodology whereas specific prescriptive guidance will be followed in subsequent subsections. By focusing on the assessment of existing Italian school buildings, this paper offers a clear and concise implementation of the methodology that can be used by practitioners wishing to make informed decisions during their assessments.

3.1. Building survey

For each school building outlined previously, an inventory of damageable structural and non-structural elements was compiled based on the information gathered during in-situ surveys. Before surveying the buildings, available information such as design documentation, certificate of the materials or non-destructive testing was collected. During the surveys, architectural drawings were used in order to verify the geometry of the buildings as well as the structural layout. The positions and dimensions of the structural elements were verified, compiling a form in which all the observations were annotated. The possible degradation or cracking of the structural elements was checked in the RC and URM buildings, while in the PC building particular attention was paid to the beam-column connections, as well as to the connection of the cladding panels to the structural elements. Furthermore, each school building was equipped with a structural monitoring system aimed to identify the modal properties of the structures through ambient vibration acquisition in addition to forced vibrations from nearby earthquakes. A forced vibration recording was triggered in the case of the RC building considered here during the 2016 Central Italy earthquake; interested reader is referred to O'Reilly et al. [24] for further details on this event.

Specific procedures were developed to inventory all non-structural elements. A preliminary analysis allowed the identification elements typically present in school buildings and for each of them, a specific form was developed in order to quantify the elements and define all the information required in loss estimation. The forms were divided into six sections. In the first general section, a description of the non-structural element was provided along with two representative photos; one providing an overview of the element while the other showing information about the anchorage of the non-structural element to the supporting structure. In the second section, the location and quantity of the non-structural elements are defined. The locations were defined looking at the floors and the rooms where the non-structural elements are located. Different units are used to quantify the non-structural elements; m^2 are used for ceiling systems while the bookshelves are quantified by number of units, for example. The third section is aimed to define a safety index for the specific non-structural element analysed in the form. To define a safety index, a questionnaire mainly related to the anchorage with the supporting structures is included. This section is useful to define a preliminary evaluation of the seismic risk for the non-

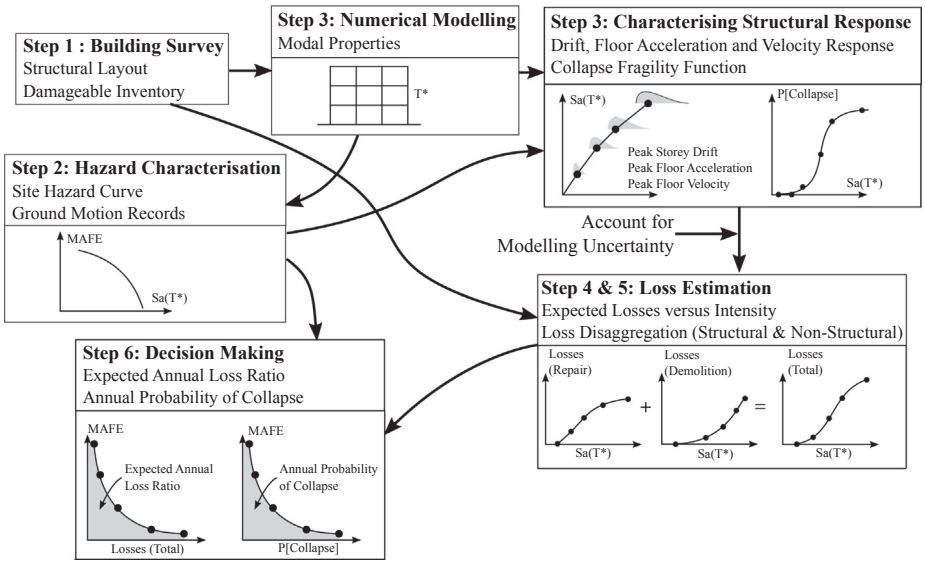

Fig. 3.1. Overview of assessment methodology employed for school buildings with reference to the PEER-PBEE methodology.

structural elements. In the literature, some rapid visual screening methodologies based on questionnaires are available and used to create a priority list that helps identify the more critical buildings and where more detailed analytical investigations should be applied, both from a structural and non-structural point of view [25,26]. In the fourth section of the questionnaire, some typical retrofit strategies for the non-structural elements proposed by published codes and some guidelines [27,28] are identified. The seismic details indicated in this section are compared with the non-structural details available in the buildings in order to define the safety index associated with each non-structural element typology. Finally, the last two sections are used to provide all the information required for the loss assessment. This part of the form was not completed during the survey but is required for the loss estimation analysis. In particular, the data related to the fragility and consequence functions must be specified. More details about the fragility and consequence functions used in this study are provided in Section 3.5.

3.2. Numerical modelling

Using the structural layout and material property information identified during the building surveys, a non-linear numerical model of each school building was developed to identify both modal properties required for the ground motion record selection and seismic response characterisation outlined later. This response characterisation will then serve as the input to the loss estimation study in the following steps so that the direct economic losses can be estimated for each building.

In the case of the RC school building with masonry infill (see Table 2.1), the model was developed in OpenSees [29] following the recommendations of O'Reilly and Sullivan [30] for older RC frame structures in Italy. Fig. 3.2 illustrates the main elements of the numerical model for the RC school building. The beam and column elements were modelled using the force-based beam-column element with a Modified Radau plastic hinge integration scheme [31] to give a lumped plasticity element. The flexural behaviour accounted for the post-peak strength and stiffness degradation of the members, in addition to the increased pinching in the hysteretic behaviour to allow for the eventual flexural failure of the members, as illustrated in Fig. 3.2. The shear response of the column members was modelled by introducing an uncoupled zero-length element at the member ends. These elements were modelled using the model proposed by Zimos et al. [32] to account for the potential shear failure in these members as a result of excessive shear force transfer from the masonry infills or staircases. The potential loss of vertical load-carrying capacity of the column or beam-column joint members through excessive shear damage was not explicitly modelled due to limitations in the element formulation that do not allow for axial, shear and flexure interaction. Some more advanced elements are being developed (e.g. [33]) but can be computationally expensive and restrict the explicit definition of specific aspects of non-ductile RC column behaviour (e.g. plastic rotation capacity and post-peak degradation) handled here through the definition of lumped plasticity elements. The presence of smooth bars was noted the in-situ testing report provided during the visit to the school and, therefore, the hysteretic behaviour of the elements was defined using the recommendations of O'Reilly and Sullivan [30] that accounts for this effect. Information required to model the beam and column members was taken from the available survey reports, where details regarding material properties and reinforcement content was provided for a number of members. For members that had no available information, a reasonable value was estimated through simulated design calculations. The approach adopted to model the behaviour and capture the effects of beam-column joint on the overall frame response is also illustrated in Fig. 3.2, where each joint region was modelled using a zero-length hinge element to capture the non-linear behaviour and rigid offsets to represent the physical dimensions of the joint. The floor slab system was assumed to be rigid following the examination of the actual floor system in place, which is a *laterizio* system [34]. This floor system was quite common in Italy for RC buildings built in the 1960s. Based on engineering judgement, such a floor system was not deemed flexible enough to have a great impact on the structural analysis results and was therefore assumed rigid for simplicity. The stairs system was modelled using a series of elastic frame elements to account for the potential shear failure of the surrounding columns, in addition to accurately modelling all sources of lateral stiffness so as to adequately capture the torsional modal behaviour of the school, as outlined in O'Reilly et al. [35]. The exterior masonry infill wall was identified as double leaf hollow clay brick masonry and was modelled using an equivalent diagonal strut approach [36] with the "medium" strength material properties provided in Hak et al. [37].

The URM school building (see Table 2.1) was modelled using

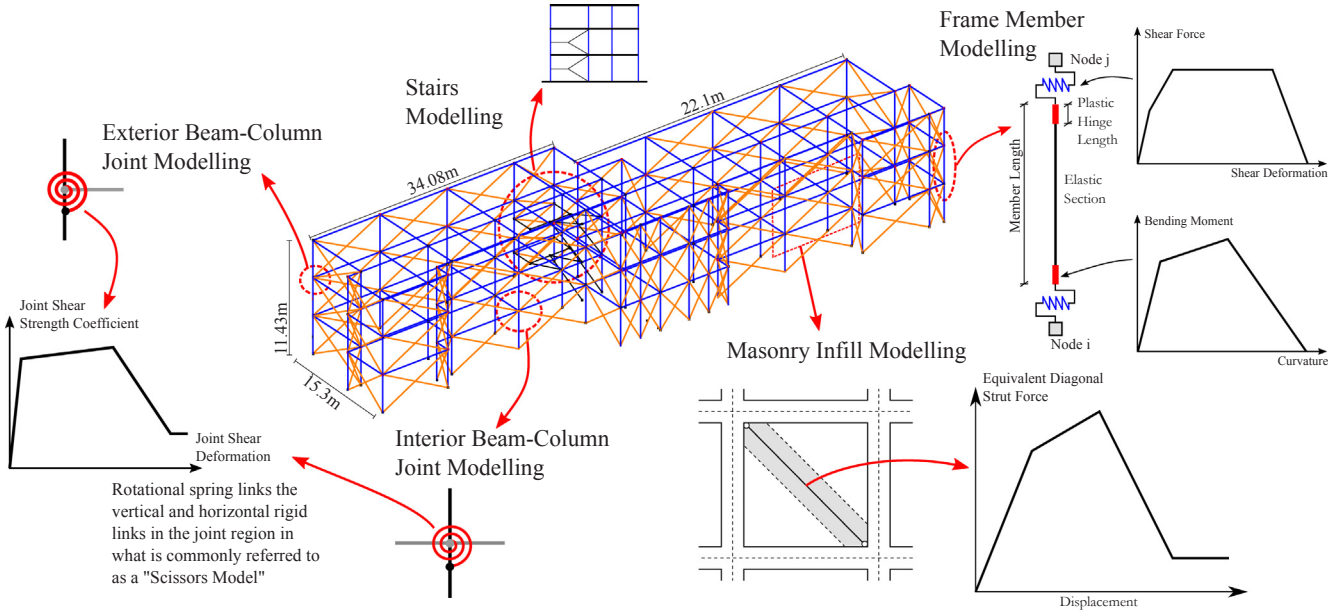

Fig. 3.2. Illustration of the numerical modelling of the RC building where the various details regarding the modelling of RC frame behaviour are highlighted. For further details on element modelling, see O'Reilly and Sullivan [30].

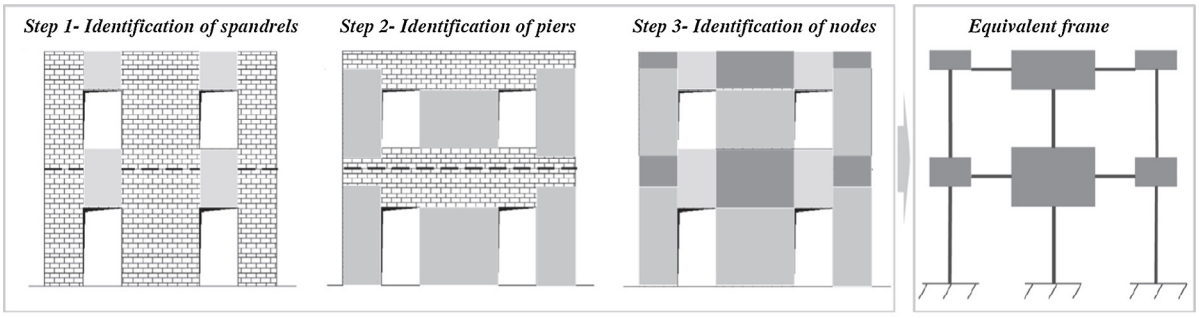

(a) Equivalent in-plane frame idealisation of the URM walls using TreMuri for masonry structures (adapted from Lagomarsino *et al.* [38]).

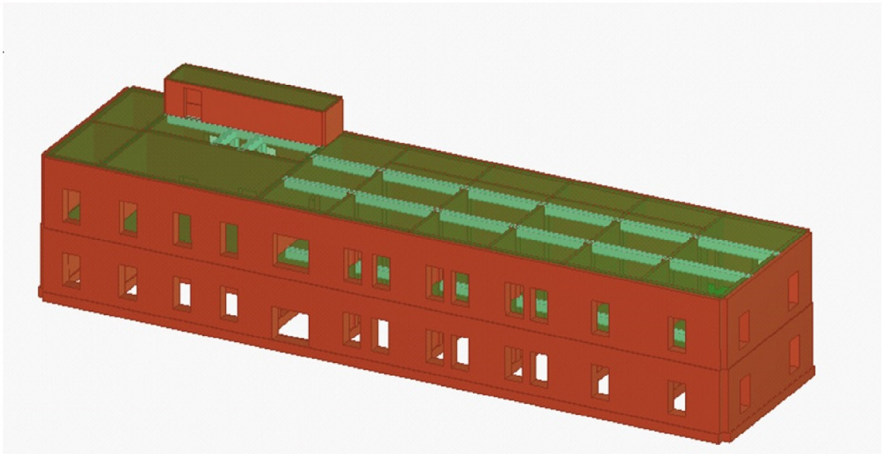

(b) Isometric view of URM school building modelled using TreMuri.

Fig. 3.3. Numerical modelling of URM school building using TreMuri. (a) Equivalent in-plane frame idealisation of the URM walls using TreMuri for masonry structures (adapted from Lagomarsino et al. [38]). (b) Isometric view of URM school building modelled using TreMuri.

TreMuri [38], which allows for the evaluation of both local and global seismic response of URM buildings. The structural model was developed using the equivalent frame approach. Fig. 3.3(a) summarises the steps required to define the idealised equivalent frame model and Fig. 3.3(b) shows an isometric view of the school building model developed. Using this approach, a generic masonry wall with opening is idealised by identifying two main structural components: the piers and the spandrels. The piers are the main vertically resisting elements while the spandrels couple the response of two adjacent piers. This methodology was developed from the observation of typical damage during past earthquakes [38]. The identification of the geometrical properties of piers and spandrels is automatically performed by the software according to conventional criteria. The non-linear macro-element model implemented in TreMuri allows the two main failure modes governing the response of masonry walls to be reproduced with a limited number of degrees of freedom. In terms of flexural behaviour, rocking and crushing mechanisms are considered, whereas diagonal cracking and shear sliding are taken into account for shear failure. In order to define the ultimate shear and bending strength, simplified criteria are implemented in the software. The elastic behaviour is defined considering the mechanical and geometrical properties of the masonry and a stiffness reduction factor is introduced to account for cracked conditions. The maximum capacity in compression is limited to $0.85 \cdot l \cdot t f_u$, where l is the length of the cross-section, t the thickness of the wall and f_u the masonry compressive strength. For the shear failure mechanisms, the Coulomb criteria is taken into account. The failure of the panel is based on a limiting storey drift value defined from the governing failure mode and according to code prescriptions [22,39]. If the maximum storey drift in a pier is achieved, the element becomes a strut, which means no residual shear and bending capacity is assumed while the axial load is still carried.

Finally in the case of the PC school building, the numerical model was developed using Ruaumoko3D [40]. The structural system comprises precast columns that support precast beams in the longitudinal direction only, as illustrated in Fig. 3.4(a). For the precast columns, a lumped plasticity modelling approach was adopted, using Giberson one-component plastic hinge members [41]. Plastic hinges were able to form at both ends of the columns in both storeys, with the plastic hinge length being calculated using the empirical expression given by Paulay and Priestley [42]. Given the limited strength of the beam-column joint and lack of moment transfer between the column and beam, plastic hinge formation was deemed not possible in the beams and they were hence modelled as linear elastic frame elements. The hysteretic behaviour of the plastic hinges in the columns was modelled using the Takeda hysteresis rule [43] with the unloading and reloading parameters, α and β, set to 0.5 and 0.0, respectively [40]. This results in a 'thin' moment–curvature hysteresis suitable for representing the behaviour of reinforced concrete columns [44]. Beam-column joints represented the most complex element of the PC. The in-situ surveys of the school building, outlined in Section 3.1, showed the beams were seated atop the column corbels without any additional restraint. No dowel-type connections or neoprene pads were observed in the joint, only mortar packs. To capture the expected behaviour, the joint was modelled as shown in Fig. 3.4(b). The depth of the beam was modelled using rigid frame elements, which at the underside of the beam connect to a friction element that allows for sliding between the beam and column corbel. Gap elements were then provided at both the top and bottom of the beam to model the contact between the end of the beam and the

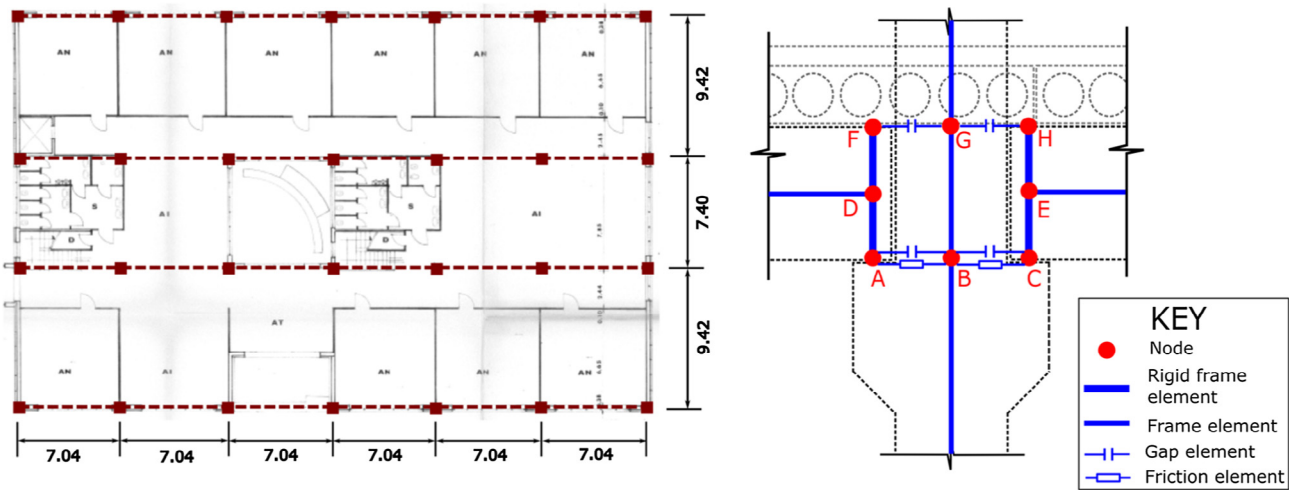

(a) Plan layout highlighting the location of beams in red (All dimensions in m).

(b) Modelling of beam members seated on column corbels using gap and friction elements.

Fig. 3.4. Illustration of the numerical modelling of the PC building. (a) Plan layout highlighting the location of beams in red (All dimensions in m). (b) Modelling of beam members seated on column corbels using gap and friction elements. (For interpretation of the references to colour in this figure legend, the reader is referred to the web version of this article.)

column face. Dynamic sliding was modelled at each joint and seating failure was assumed to occur when the beam displacement relative to the corbel exceeds the seating length. This was not explicitly modelled but was checked during post-processing of the results. Due to the precast floor topping being thin, it was decided to model explicitly the flexibility of the diaphragms, rather than assuming a rigid diaphragm. During in-situ inspection, it was deemed via engineering judgement that the connection of the cladding panels was insufficient to have any significant impact on the lateral behaviour and was therefore not considered explicitly in the numerical model.

Other aspects regarding the modelling of the three buildings were also needed for dynamic analysis and response characterisation, as discussed later in Section 3.4. The first regarded the incorporation of the second-order geometry effects of the gravity loading, or P-Δ effects, which have been incorporated in each model by applying the tributary loading collected from each floor slab and beam onto the corresponding column for each of the building typologies considered. These loads were applied as a constant load before the dynamic analysis and maintained throughout the analysis to incorporate their effects on the response of the structure. The elastic damping in the PC and URM structures was defined through a 5% tangent stiffness proportional Rayleigh damping model. For the RC building modelled using OpenSees, a modal damping model [45] was adopted by applying a constant 5% of critical damping to all modes of vibration. This damping model, when combined with the adopted beam-column formulation outlined above, has the benefit of mitigating the introduction of potential errors highlighted by Chopra and McKenna [45]. Cracked section stiffness was assumed when modelling the structural elements of each school building. For RC members, this was modelled as a constant stiffness to the nominal yield point, whereas the URM elastic modulus was based on code recommended coefficients [22]. This was done to better represent the building behaviour into the non-linear response range and to adequately capture the strength and stiffness degradation at more critical limit states. More advanced modelling techniques to include the initial elastic member stiffness followed by a reduction of stiffness upon cracking may also be adopted, but are computationally expensive typically. O'Reilly et al. [35], for example, investigated the impact of this initial stiffness modelling on storey drift and floor acceleration demand for the RC building outlined here. The response of the initially uncracked model was shown to converge toward the initially cracked section stiffness model at relatively low levels of intensity. As such, this discrepancy at low levels of shaking should not impact the overall conclusions of the work presented herein.

3.3. Characterisation of site hazard

As discussed in Section 2, the school buildings considered here were constructed prior to the introduction of modern seismic design provisions in Italy; which prescribed specific detailing rules regarding material properties and minimum amount and arrangement of longitudinal and transversal reinforcement in beams and columns [46]. Moreover, the selected schools are anticipated to be representative of the Italian school building stock, based on statistical information collected and outlined in Borzi et al. [1]. Information on each school building is listed in Table 2.1 and their main characteristics are sufficiently general to be considered representative of the overall school building stock (i.e. structural layouts and building materials were not specific to any particular region). Therefore, it was assumed reasonable to expect school buildings of similar constructions to be built at different locations throughout Italy. It was thus decided that each school building analysed may exist at any given location throughout Italy and that a number of site locations could be considered to analyse these buildings. As such, two site locations were chosen to perform probabilistic seismic hazard analysis (PSHA) and select hazard-consistent ground motion record sets: the cities of Ancona and Cassino, which may be assumed to represent and be herein referred to as medium and high seismicity in Italy, respectively. This not only allowed the number of case study applications of the PEER-PBEE methodology to be doubled, but also illustrate the relative differences between the building seismic performances in areas of different seismicity. This type of information may be useful for governing bodies looking to prioritise the allocation of limited economic resources in order to reduce the seismic vulnerability of an entire territory through retrofitting of these typologies located in areas of different seismicity. This consideration is beyond the scope of this article, but it is noted that such information may be used to further develop prioritisation schemes similar to that conducted by Grant et al. [47] that can aid in inferring a level of vulnerability and establish a decision-making framework. The difference being that the prioritisation may be based on economic vulnerability rather than discrepancy in peak ground acceleration used during design and that prescribed by modern seismic hazard maps [47]; if any consideration was indeed given to horizontal ground accelerations. Therefore, by considering

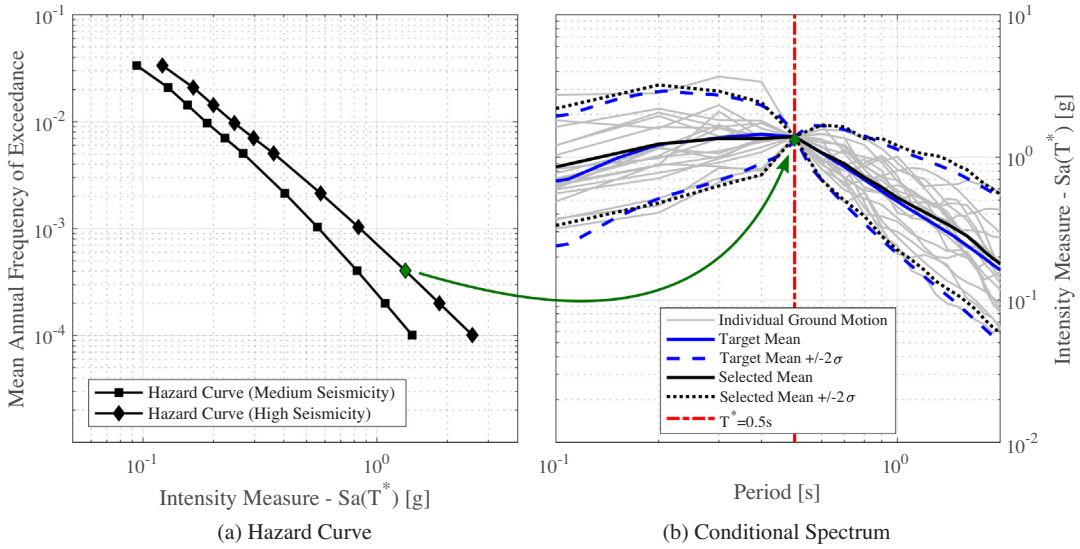

Fig. 3.5. Illustration of (a) the site hazard curve for both sites at a conditioning period of $T^* = 0.5$ s and (b) an example of the ground motion records selected at the high seismicity site, where the target conditional spectrum is shown relative to the selected ground motion set. Note: the selection in (b) shows the 2475-year return period records selected with a modal contributing scenario of M = 6.25, Distance = 10 km and epsilon = 1.25.

more case study applications via different site locations and seismicity levels, this information may be used to refine future prioritisation schemes by using economic losses as the decision-making metric rather than design input acceleration deficiency.

The procedure illustrated in Fig. 3.5 was used for the selection of ground motion records to match the conditional spectrum [48,49] at different return periods. The selection was based on the modal value of the contributing scenarios obtained from disaggregation of the PSHA results. A total of 20 pairs of ground motion records (consisting of two horizontal components) were selected at 11 return periods for both sites with Soil Type C, as defined by Eurocode 8 [50]. The intensity measure (IM) chosen to characterise the response of the buildings was the spectral acceleration, $Sa(T^*)$, at a conditioning period, T^*. Each building possesses a principal mode of vibration in the two orthogonal directions (Table 3.1) therefore, a suitable value of T^* needed to be established. FEMA P58 [23], for example, suggests adopting a T^* equal to the arithmetic mean, or average, of these two orthogonal modal periods. Another issue to consider was the hazard data at the two sites investigated, which was available at a discrete number of vibration periods. As such, the adopted approach was to compute the average of the period in both orthogonal directions, $T_{average}$, and then adopt the closest T^* from the periods for which PSHA information was available, all of which are listed for each school building in Table 3.1. Since hazard consistent record selection was performed and considering the findings of Lin et al. [51], this discrepancy in T^* and the first mode vibration period is deemed a reasonable approximation. The ground motions were taken from the PEER NGA-West 2 database [52], carrying out a hazard-consistent record selection based on the spectral compatibility with the geometric mean spectrum using the methodology outlined in Jayaram et al. [49], which also considers the conditional variance of the spectral acceleration away from the conditioning period. The selection criteria considered the spectral acceleration as the maximum between the two as-recorded component pairs, which is consistent with the ground motion prediction equation by Ambraseys et al. [53] employed here for the hazard calculations. The seismic hazard calculations and the derivation of the conditional mean spectrum were performed using the REASSESS software tool [54], using the spectral acceleration correlation model proposed by Baker and Jayaram [55]. A maximum scaling factor of 4.0 was imposed to avoid excessive scaling, with the exception of the 4975 and 9975-year return periods where scale factors up to a value of 8.0 were considered.

Table 3.1
First mode periods from numerical models and adopted conditioning periods.

School	Longitudinal mode period ($T_{1,X}$)	Transverse mode period ($T_{1,Y}$)	Arithmetic mean ($T_{average}$)	Conditioning period (T^*)
RC	0.62 s	0.36 s	0.49	0.50 s
URM	0.42 s	0.23 s	0.32	0.20 s
PC	1.19 s	1.16 s	1.17	1.00 s

3.4. Characterisation of structural response

Following the modal analysis and ground motion selection, a series of non-linear response history analyses (NRHA) were conducted using multiple-stripe analysis (MSA) [56]. In addition, pushover analyses were conducted to characterise the static response of the school buildings and are shown in Fig. 3.6. The points at which each of the limit states discussed in further detail in Section 4.3 are exceeded are also indicated on each pushover curve. In MSA, a set of ground motion records is selected in correspondence with the available hazard disaggregation at the conditioning period to evaluate the building response at increasing levels of intensity and return period. Fig. 3.7 illustrates the response curves conditioned on no structural collapse for each of the school buildings using the ground motion records from both site locations. Each dot represents the median of the maximum values of peak storey drift (PSD) or peak floor acceleration (PFA) up the height of the building in a single direction for a given return period. This way, the evolution in median peak storey drift and floor acceleration with respect to intensity for the different structural typologies can be observed. Some preliminary observations of the results presented in Fig. 3.7 are that in terms of median peak storey drift demand, the RC and PC frames are much more flexible that the URM building, with the median peak storey drift demand profiles exceeding 2% of the storey height for the higher return periods. Between the RC and PC frames, the RC frame is much stiffer due to the presence of the masonry infills, also seen through the first mode periods of the buildings in Table 3.1. This is also reflected by the higher PFA profiles for the infilled RC frame. It is noted for completeness that Fig. 3.7 illustrates the median peak profiles for each of the 20 ground motion records conditioned on no collapse, whereas the associated uncertainty due to record-to-record variability is

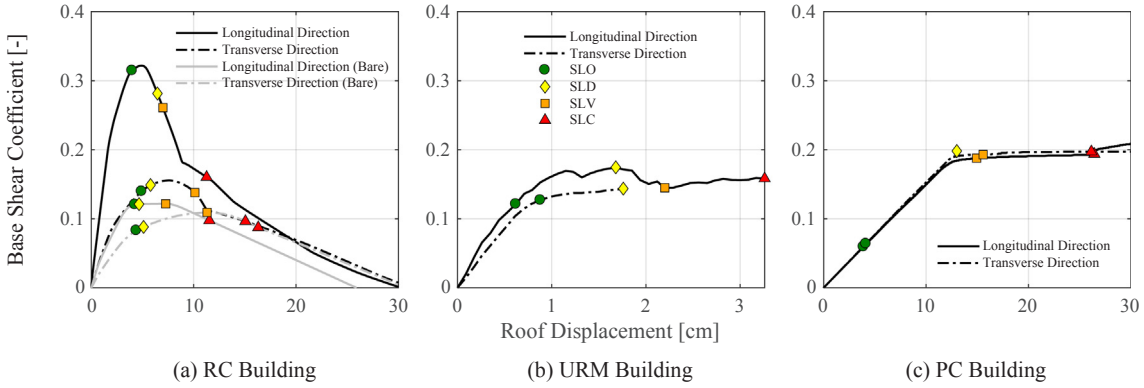

Fig. 3.6. Static pushover curves for each of the school buildings, where the base shear has been normalised by the total building weight and the point at which each of the limit states are exceeded.

also documented and maintained as input for the loss estimation computations discussed later.

While the results presented in Fig. 3.7 describe the median response conditioned on no structural collapse, the actual collapse performance is also required to compute the total expected losses, $E[L_T|IM]$, arising from both the collapsing and non-collapsing cases, according to Eq. (3):

$$E[L_T|IM] = E[L_T|NC,IM](1-P[C|IM]) + P[C|IM]\cdot RepC \quad (3)$$

where $P[C|IM]$ represents the probability of collapse for a given level of IM, the labels C and NC denote the collapse and no collapse cases, respectively, and RepC represents the replacement cost of the building.

By counting the number of ground motion records that resulted in the prescribed collapse criterion being met at each intensity level, the probability of collapse was computed at discrete intensity levels. The term collapse refers herein to the complete loss of lateral and vertical load carrying capacity at one or more storeys of the building and does not incorporate any aspects related to post-earthquake decisions to demolish the building due to excessive damage or residual drift as those will be treated separately in Section 3.6. Using this information, a continuous lognormal distribution was fitted to the data to describe the probability of collapse with respect to intensity. This was done by establishing an appropriate median collapse intensity, θ, and logarithmic standard deviation, β_{RTR}, value associated with record-to-record variability using the maximum likelihood method outlined by Baker [57]. Guidelines such as FEMA P695 [58], for example, propose adjustments to the median and dispersion values of the established collapse fragility function to account for the effects of spectral shape on the collapse performance. However, as the ground motion records selected

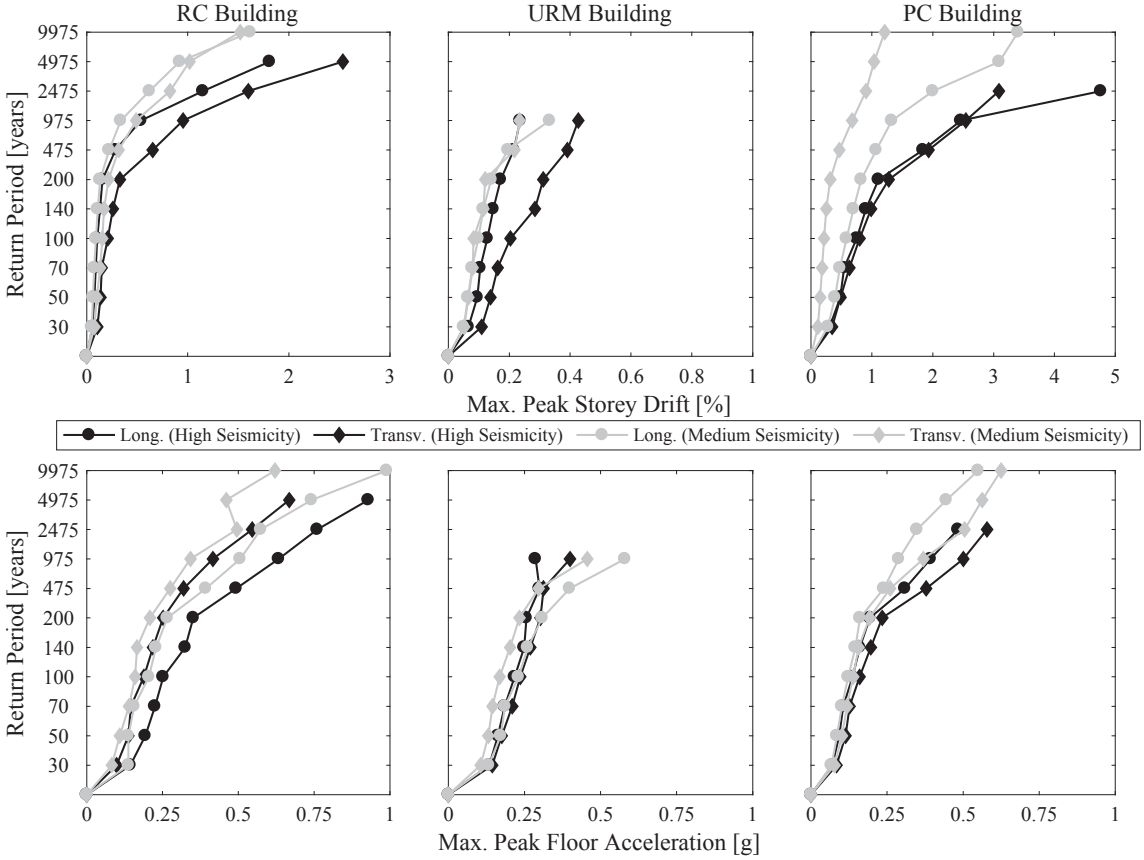

Fig. 3.7. Median of the maximum values over the height for peak storey drift and peak floor acceleration in both longitudinal and transverse directions of the case study school buildings using the ground motion records for both site locations.

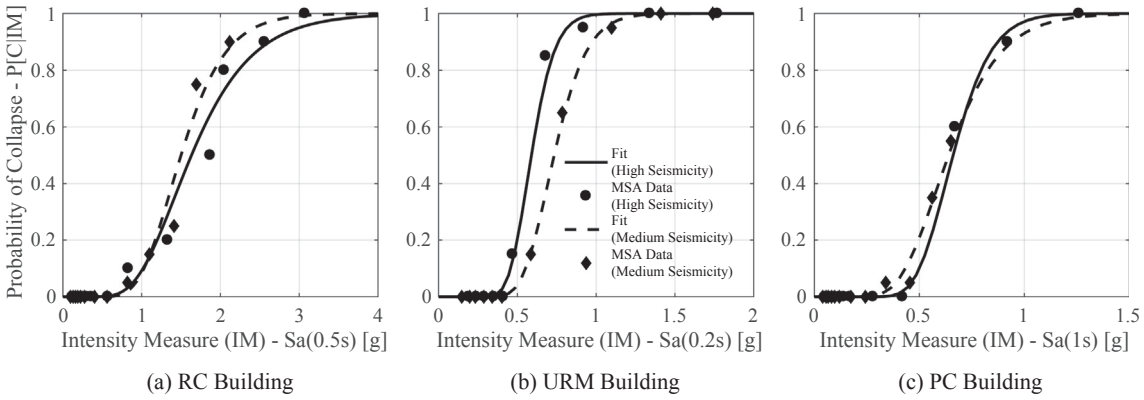

Fig. 3.8. Collapse fragility functions for each of the case study school buildings for both sets of ground motion records.

here were consistent with PSHA information at each intensity level, no such adjustment was necessary as spectral shape effects were inherently taken into account.

For the RC frame building with masonry infills, the collapse criterion was defined as when the PSD exceeded 10% at any level of the building in either direction. This does not necessarily imply that the RC building may be expected to sustain drift demand of up to 10%. It serves as a quantitative definition in order to confidently state that the building model has reached its limiting intensity for a particular ground motion (i.e. the building's lateral drift response tends toward infinity, referred to as flat-lining in IDA [59]) by accumulating excessive lateral drift at one or more levels. This aspect has been discussed in detail by O'Reilly et al. [60] who, by varying the collapse criterion definition, demonstrated that the median and dispersion of the collapse fragility function; developed using this quantitative partitioning of collapse and non-collapse cases, tended to stabilise for a PSD limit exceeding ~5%. This was also strengthened by the proposals of Rossetto and Elnashai [61] who, from past earthquakes and numerous experimental test campaigns, suggested that the collapse of non-ductile RC frames with masonry infill is anticipated from a drift of 4.36% onward, which resonates with the above numerical study. Therefore, the collapse criterion used here could have been set at 5% with little or no consequence to the subsequent collapse fragility function. To have a more populated collapse dataset, some additional intensity stripes were analysed to estimate the collapse probability at increasing return periods. This was done by scaling the 9975-year records up by 1.2 and 1.5 in the case of the medium seismicity site and by 0.8 and 1.2 for the high seismicity site in the case of the RC building. This resulted in a more populated empirical dataset with which to fit a lognormal distribution, compared to the collapse data obtained from the original ground motion set that lacked collapse occurrences in some intensity regions, resulting in a somewhat sparse dataset. As such, this scaling of ground motions for the purposes of fitting a collapse fragility was deemed acceptable since the dispersion was markedly reduced in both cases.

For the URM building, collapse was evaluated by examining the failure of pier elements by shear or flexure mechanism. For the building examined here, failure occurred in shear in all cases and therefore the NRHA results were checked for the exceedance of a drift limit corresponding to the shear failure of the piers. The Italian national code [22] specifies this storey drift limit as being 0.4% for pier members forming a mechanism in shear at the ultimate limit state. However, examining the data presented in Ottonelli et al. [62] and Morandi et al. [63], which also form the basis of the fragility functions adopted in the subsequent section, it was deemed that this 0.4% limit may be conservative when referring to complete collapse. Accordingly, in line with the objective of evaluating the actual collapse of the pier elements and therefore of the building, a drift limit of 0.5% was adopted in this study to define the collapse of the URM building, as it corresponds well with the drift for the loss of capacity described in Ottonelli et al. [62]. In the case of the PC building, three collapse modes were considered: column shear failure, column flexure failure (i.e. excessive plastic hinge rotation) and beam unseating from the column corbel. These failure modes were not accounted for in the numerical model but rather were incorporated through post processing of the MSA results, where exceedance of either one resulted in that run being marked a collapse case. Analysing the relative movement of each joint during dynamic analysis, it was observed that the unseating of the beam members from the column corbel was not the critical collapse mechanism in any case. To identify vertical collapse of the structure due to column failure, the plastic hinge rotation was checked against the capacity computed using the model proposed by Haselton and Deierlein [64]. Although the PC building was constructed without any modern seismic design provisions, it was noted that deformed bars were used in the precast members, hence the use of Haselton and Deierlein [64] was deemed reasonable. This capacity considers the ductile flexural failure of the member and represents the point of maximum force prior to the degradation of the member strength. The shear capacity of the columns was calculated using the model developed by Priestley et al. [65] and was compared with the column shear demand during the post-processing of the analysis results also. The exceedance of either of these two criteria in the columns was assumed to cause loss of vertical load carrying capacity, although this may be considered a somewhat conservative assumption.

Using the above criteria and general approach, Fig. 3.8 shows the resulting collapse fragility data and fitted log-normal probability functions for each case study school building at both site locations described in Section 3.3. The median, θ, and logarithmic standard deviation, β, describing the fitted log-normal collapse fragility functions are listed in Table 3.2. The fragility functions are not directly comparable between buildings due to their differing IMs and would need to be integrated with the associated hazard curves in order to make a meaningful comparison. The collapse fragilities for each school building at the two site locations are relatively consistent between the two different record sets utilised. It is noted that for the PC building, although the median collapse intensities are similar, the dispersion for the medium seismicity site is larger than that of the high seismicity site. This may be as a result of many different aspects of the approach

Table 3.2
Median collapse intensities, θ, and dispersion due to record-to-record variability, β_{RTR}, for each case study school building.

School building	High seismicity		Medium seismicity	
	θ	β_{RTR}	θ	β_{RTR}
RC	1.63 g	0.37	1.50 g	0.29
URM	0.59 g	0.20	0.73 g	0.22
PC	0.66 g	0.22	0.64 g	0.30

adopted here, such as fitting methodology, completeness of collapse dataset, ground motion sets and adopted intensity measure, which are deemed beyond the scope of this article.

3.5. Identification of damageable inventory and fragility and repair cost functions

Before conducting loss estimation, a building performance model is required for each school building. As defined in FEMA P58 [66], a building performance model is an organised collection of data regarding all structural and non-structural elements that could be damaged during an earthquake. An inventory of all damageable structural and non-structural elements was defined for each building using the information collected during surveys and the available documentation outlined in Section 3.1. The non-structural forms filled during the surveys allowed for the accurate evaluation of all damageable non-structural elements and for the assessment of their protective systems, both for acceleration and drift-sensitive elements. If the information regarding the protection of the non-structural elements was not available, these elements were intentionally considered as having no seismic design provisions. This was done to be more representative of the observed non-structural detailing in older Italian buildings. Table 3.3 reports a list of all damageable structural and non-structural elements considered in this study for each school building typology examined. The quantities are expressed using different units based on the element typology. For each typology, Table 3.3 reports the demand parameters, quantities and references used to define the fragility and consequence functions. For structural elements, the assumed demand parameters are the PSDs for RC and PC buildings, and the element chord rotations for the URM building. For the PC building elements, fragility and consequence functions for the precast columns and panels were determined through consultation with practitioners in Italy. For non-structural elements, the main demand parameters are the PSDs, peak floor velocities (PFVs) and PFA. Once the demand parameters are defined, the likely damage that will be experienced by the damageable elements is computed using the fragility functions associated with each of the sequential damage states. The selection of more representative fragility functions is a complex issue and is one of the main problems related to the accurate estimation of earthquake-induced losses. The main issue concerns the availability of adequate fragility functions for all the elements in the building and this is often related to the non-structural elements for which few experimental studies are available; hence, some assumptions were required.

The adopted fragility function sources are reported in Table 3.3. For the RC building elements, existing fragility functions [67,68] were adopted, while for the URM building, the experimental data described in Morandi et al. [63] was utilised. Failure of masonry components is based on the chord rotations, whose fragility functions are distinguished between flexural and shear failure of the pier elements and also between the type of lintels present in the spandrel elements. This differentiation between failure mode of the pier elements and lintel typology of the spandrel elements was also maintained for the repair cost functions adopted from Ottonelli et al. [62]. In terms of non-structural elements, the fragility functions proposed by Sassun et al. [69] were adopted for the masonry infills, while those proposed in FEMA P58 were assumed for all acceleration and velocity-sensitive non-structural elements. For some non-structural elements, specific fragility functions were not available thus some assumptions were made using engineering judgement. For example, the fragility functions of the desks and chairs were correlated to the fragility functions assumed for the partition walls, considering that the collapse of the partition walls would damage the adjacent desks and chairs. The repair costs included all the construction activities necessary to return the damaged components to their pre-earthquake condition. Repair times and casualties were not taken into account in this study. For the structural elements of the RC building, existing consequence functions [67,68] were utilised, while for the URM building the consequence functions proposed by Ottonelli et al. [62] were used to maintain consistency with the fragility functions set previously described. For the PC building the repair costs were estimated referring to the Italian costing manuals [70]. For many non-structural elements, the assumed fragility and repair cost functions were taken from the Performance Assessment Calculation Tool (PACT) fragility library [66], which has been largely developed for use in the US. In order to make the repair cost functions applicable to older Italian buildings examined here, an equivalent conversion between average construction costs in the US and Italy for the year 2013 was utilised, where Italian costs were 1.22 higher on average. For cases where no costing information was available, expert opinion was sought from an Italian consulting engineering firm. Therefore, the term “Expert Opinion” noted in Table 3.3 for various structural and non-structural elements refers to costing information that was developed explicitly in this study using costing manuals to give a cost breakdown of the various works involved in their repair.

3.6. Loss estimation

Following the characterisation of the seismic hazard and structural response, along with the inventorying of the damageable structural and non-structural elements, loss estimation was conducted for each building. The structural response characterisation was presented in Section 3.4 and illustrated in both Figs. 3.7 and 3.8 for the collapsing and non-collapsing cases, respectively. This analysis was conducted using the ground motion records identified earlier in Section 3.3 using a single deterministic numerical model. As such, no consideration was given to the fact that the numerical representation of the school buildings via modelling is not perfect and possesses its own inherent uncertainty. This is typically referred to as modelling uncertainty and is a form of epistemic uncertainty that should be considered in assessment. The only uncertainty considered thus far in the assessment has been the aleatory uncertainty associated with the record-to-record variability, β_{RTR}. To indirectly account for the additional dispersion introduced via modelling uncertainty, β_{MU}, it is typical to inflate the dispersion β_{RTR} by a prescribed amount for the PSD, PFA demand and also the collapse fragility function using a square root sum of the squares (SRSS) combination which assumes that the two sources of uncertainty are uncorrelated [71]. For the RC frame building, empirical values proposed by O'Reilly and Sullivan [72,73] were adopted to account for the increased dispersion in the PSD and PFA demand. For the URM and PC typologies, the modelling uncertainty values were, in the absence of more detailed studies, adopted from the FEMA P695 guidelines [58] for the collapse fragility functions. Based on the qualitative description of FEMA P695, a value of 0.20 was adopted for URM and 0.35 for PC when evaluating the modelling techniques is each case, whereas a value of 0.15 was used for the RC building, as per O'Reilly and Sullivan [72,73]. For the non-collapsing cases, the modelling uncertainty associated with the demand parameters were adopted from FEMA P58 [23] where the β_{MU} terms is further broken down into β_c and β_q, which represent the additional modelling uncertainties associated with construction quality and overall quality of the numerical model, respectively. For the URM typology, these were selected as 0.40 and 0.25 for β_c and β_q, respectively, based on the qualitative descriptions provided by FEMA P58 and 0.25 and 0.40 for the PC building, respectively. For both the URM and PC typologies, the SRSS combination of the β_c and β_q values resulted in an overall β_{MU} of 0.47.

In addition to the consequence functions and repair costs outlined in Section 3.5, an appropriate estimate of the replacement costs (denoted RepC in Eq. (3)) of each school building was required so that the contribution to the expected losses from the collapsing cases could be incorporated. To estimate these replacement costs, available information for Italian school buildings following the 2012 Emilia-Romagna earthquake [74] was used to find the typical cost of replacing a building per m^2 in addition to the costs of demolition and removal of debris. The

Table 3.3
List and quantities of damageable elements in each school building. Quantities in the longitudinal direction of the school building are listed with the transverse direction listed adjacent in parentheses.

Element	Demand parameter	Fragility function source	Repair costing source	Unit	Quantities						
					RC building			URM building		PC building	
					Ground	1st Floor	2nd Floor	Ground	1st Floor	Ground	1st Floor
Structural elements											
Exterior Beam-Column Joints	Drift [%]	Cardone [67]		each	20(26)	20(26)	20(26)	–	–	–	–
Interior Beam-Column Joints	Drift [%]			each	23(15)	23(15)	22(14)	–	–	–	–
Non-Ductile Columns	Drift [%]			each	44	44	44	2	2	–	–
Exterior masonry infill (double leaf, hollow clay bricks)	Drift [%]	Cardone and Perrone [68]		m^2	454.4(2.0)	454.4(127.8)	447.3(125.8)	–	–	–	–
Staircase	Drift [%]	FEMA P58-3 [66]		each	1	1	1	1	1	2	2
Precast Columns	Chord Rotation [%]	Expert Opinion		each	–	–	–	–	–	28	28
Precast Panels	Panel Moment [kNm]	Expert Opinion		each	–	–	–	–	–	6(12)	6(12)
Unreinforced Masonry Piers	Chord Rotation [%]	Morandi et al. [63]	Ottonelli et al. [62]	m^2	–	–	–	212.4 (329.1)	225.2 (370.6)	–	–
Unreinforced Masonry Spandrel	Chord Rotation [%]			m^2	–	–	–	77 (15.3)	87.5 (20.6)	–	–
Non-structural elements											
Interior Gypsum Partitions	Drift [%]	Sassun et al. [69]	Expert Opinion	m^2	317.8(335.3)	291.9(243.6)	268.1(2 3 1)	176(2 4 8)	191.4(269.7)	786.9(515.9)	537.9(391.6)
Interior masonry infill (single leaf, hollow clay bricks)	Drift [%]			m^2	198.9(65.9)	198.9(65.9)	195.7(64.8)	–	–	–	–
Doors	Drift [%]			each	18(15)	13(10)	15(10)	15(5)	13(3)	35(24)	20(17)
Windows	Drift [%]			each	23(17)	50(9)	53(9)	23(2)	26(2)	26(17)	23(13)
Desks	Drift [%]			each	110	145	182	82	104	410	393
Chairs	Drift [%]			each	140	182	182	108	134	509	469
Ceiling System	PFA [g]	FEMA P58-3 [66]		m^2	560	588	566	365	365	1651	1490
Fancoils	PFA [g]			each	28	30	30	8	10	50	35
Lighting	PFA [g]			each	66	48	48	52	56	176	142
Piping – Water Distribution	PFA [g]			m	452	452	452	232	232	763	496
Piping – Heating Distribution	PFA [g]			m	476	476	476	140	140	1330	967
Bookcases	PFV [m/s]			each	16	22	14	8	12	41	43
Mobile Blackboards	PFA [g]			each	3	3	4	11	12	29	12
Electronic Blackboards	PFA [g]			each	0	3	3	0	6	0	7
Computers and Printers	PFA [g]			each	6	20	0	3	28	3	46
Projectors	PFA [g]			each	0	3	3	0	6	0	8
Switchboards	PFA [g]			each	1	3	3	2	7	4	12

Table 4.1
Expected losses at each intensity for each of the school building typologies at both site locations considered. Intensities as which the expected loss equals the replacement cost are highlighted in bold.

Site location	High seismicity			Medium seismicity		
Building typology	RC	URM	PC	RC	URM	PC
Total replacement cost	€ 3,929,937	€ 2,075,892	€ 4,212,616	€ 3,929,937	€ 2,075,892	€ 4,212,616
EAL [€]	€ 13,839	€9902	€12,716	€ 11,152	€6839	€5646
EAL ratio [%]	0.35%	0.48%	0.30%	0.28%	0.33%	0.13%
Intensity 1–30 years	€ 42,134	€ 16,822	€ 47,899	€ 33,001	€ 3952	€ 28,514
Intensity 2–50 years	€ 90,822	€ 18,361	€ 80,088	€ 62,673	€ 9990	€ 44,665
Intensity 3–70 years	€ 146,049	€ 34,447	€ 104,108	€ 102,801	€ 11,100	€ 63,561
Intensity 4–100 years	€ 242,511	€ 57,597	€ 153,595	€ 207,535	€ 27,115	€ 79,693
Intensity 5–140 years	€ 437,500	€ 177,468	€ 227,841	€ 314,882	€ 58,280	€ 93,905
Intensity 6–200 years	€ 613,887	€ 317,312	€ 355,128	€ 546,813	€ 148,274	€ 140,183
Intensity 7–475 years	€ 1,155,626	**€ 2,075,892**	€ 948,195	€ 859,532	€ 703,615	€ 379,907
Intensity 8–975 years	€ 2,261,119	**€ 2,075,892**	€ 1,915,721	€ 1,302,232	**€ 2,075,892**	€ 719,933
Intensity 9–2475 years	**€ 3,929,937**	**€ 2,075,892**	**€ 4,212,616**	**€ 3,929,937**	**€ 2,075,892**	€ 1,288,506
Intensity 10–4975 years	**€ 3,929,937**	**€ 2,075,892**	**€ 4,212,616**	**€ 3,929,937**	**€ 2,075,892**	€ 2,151,471
Intensity 11–9975 years	**€ 3,929,937**	**€ 2,075,892**	**€ 4,212,616**	**€ 3,929,937**	**€ 2,075,892**	**€ 4,212,616**

average replacement costs using the data obtained were estimated as €1805.75 per m^2 in addition to €95.50 per m^2 for demolition and removal debris; both of which are inclusive of taxes, administrative and technical costs and the average discounts offered by construction companies. In addition to the replacement cost of the building, a threshold value defining the ratio of expected direct loss to the replacement cost for which the stakeholder would elect to demolish rather than repair the existing, heavily damaged building, must be defined. FEMA P58 [23] suggests a value of 40%, although Cardone and Perrone [75] recently noted that when examining actual reconstruction data following the 2009 L'Aquila earthquake in Italy [76], higher cost ratios of between 60% and 75% of the replacement cost were reported. Using this information, a threshold value of 60% was adopted for all analyses discussed herein. This value considers the ratio of the direct losses to the overall replacement cost, whereas if the indirect losses and other legislative factors were to be considered, this value could be expected to be somewhat lower [77].

Residual drifts were also incorporated for the RC and PC building typologies by adopting a residual drift fragility function with a median value of 1.5% maximum residual storey drift with a dispersion of 0.30, as per Ramirez and Miranda [78]. This was used to identify situations where the permanent lateral drifts that remain following an earthquake were likely to result in the building being demolished. Therefore, in addition to the structural collapse of one or more level of the building and the accumulation of excessive expected monetary losses, the presence of excessive permanent lateral deformations is also used a criterion with which to decide if the building ought to be replaced. Residual drifts were not considered for the URM building, as to the authors' knowledge, no information similar to that outlined in Ramirez and Miranda [78] currently exists for URM structures. As mentioned in Section 3.4, the incorporation of a loss threshold and consideration of residual drifts means that in addition to a complete structural collapse at one or more storeys, other decisions taken by the building owner or local authority post-earthquake that may result in the loss and demolition of the building are treated separately. This is to avoid adopting collapse fragility function definitions that intend to anticipate demolition due to excessive damage without the structure having actually collapsed. This merging of the two motivations to demolish and replace a building may potentially result in overly conservative predictions of structural collapse and subsequently casualties as excessively damaged buildings will also result in loss of life by this definition. Villar-Vega and Silva [79] noted that such a conservatism in collapse fragility functions led to the number of casualties being heavily overestimated when compared to actual statistics following past earthquake events in Latin America, for example. Furthermore, Kim et al. [80] recently reported from the lessons learned following the 2011 and 2012 New Zealand earthquakes that the factors influencing demolition are numerous and remains an area that require further developments. Using the information outlined here and in the previous sections, the loss estimation was implemented for each of the school buildings following the assembly-based procedure. The PACT software [66] provided with the FEMA P58 guidelines was utilised here to conduct the loss estimation, which follows the basic procedure illustrated in Fig. 3.1. A total of 200 realisations were used per intensity level and the non-directional conversion factor was assumed to be 1.2. These realisations are needed to randomly sample from the input demand distributions to create a new set of demand data that accounts for modelling uncertainty through an amplified dispersion. The non-directional conversion factor is also needed when evaluating the demand on elements sensitive to damage in all directions since, to account for the fact that the actual maximum may not actually be in either principal direction.

4. Assessment results

4.1. Loss estimation

By following the procedure outlined in the previous section with the necessary information collected for the various stages of the PEER-PBEE assessment framework, loss estimation was conducted using PACT and the results for each typology at both site locations are presented and discussed in this section. For each of the 11 return periods considered, the expected loss from damage resulting from damage to both the structural and non-structural elements, in addition to losses due to collapsing cases and demolition due to excessive residual drift were computed. The total losses are reported in Table 4.1 and the ratio to the replacement cost of the building is plotted in Fig. 4.1(b) against return period for relative comparison. The expected losses reach the replacement cost at different return period intensities and is particularly notable in the case of the URM building typology for the 475-year return period event in the high seismicity zone. For the RC school typology, the losses accumulate more gradually than those of the URM counterpart to result in a complete loss of the building at the 2475-year return period for both site locations. Lastly, the PC school building typology accumulates losses gradually with respect to return period but exhibits rather different vulnerability curves for the two site locations compared to the other typologies.

The EAL was computed for each case study building; by integrating the vulnerability curve with the site hazard curves for both locations as per Eq. (2), and are reported in Table 4.1 and Fig. 4.1(a). The impact of the difference in seismicity of the two site locations is immediately evident, as the EAL values for the medium seismicity site are notably lower than those of the high seismicity site. Between the different

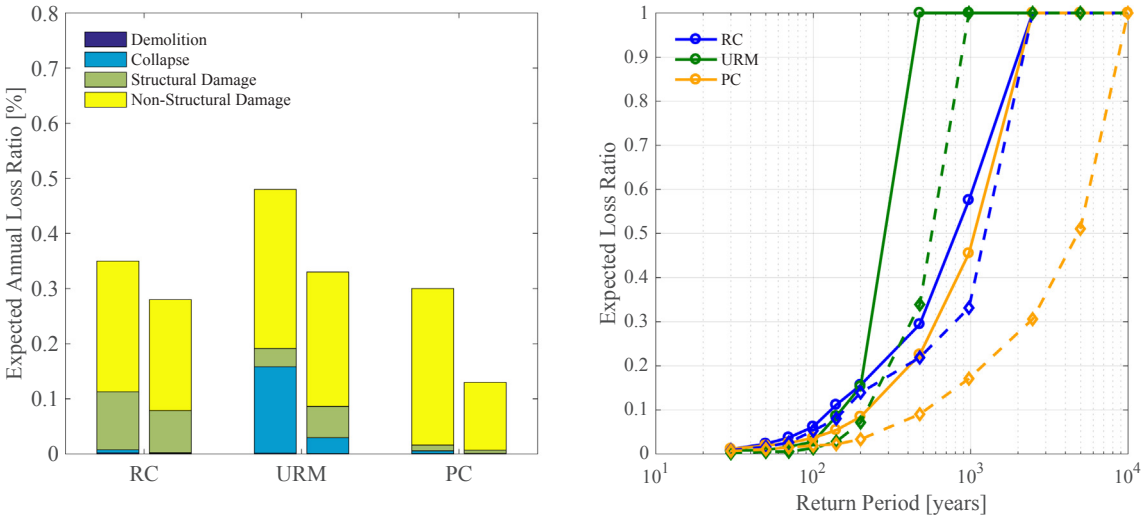

(a) Expected annual loss ratio (b) Vulnerability curves

Fig. 4.1. Expected annual loss ratio and seismic vulnerability curves for each of the school building typologies at both site locations considered. Note: (a) shows the breakdown between the different contributors and the bars on the left and right for each typology correspond to the high and medium seismicity site values, respectively, whereas (b) plots the high and medium sites as solid and dashed lines, respectively.

typologies, however, it is noted from Fig. 4.1(a) that the URM building typology appears to be the most vulnerable followed by the RC and PC buildings. Comparison can be made with some of the recent work carried out in Italy as part of one of the ReLUIS (www.reluis.it) research lines characterising the seismic performance of existing Italian building typologies. Among these typologies are pre-1970 RC frames, URM buildings and PC frames. Cardone and Perrone [75], for example, examined the performance of an existing RC frame building with masonry infill located in L'Aquila and reported EAL values between 0.75% and 1.07% depending on the assumptions made regarding the replacement cost of the building. It is noted that L'Aquila is a much higher seismicity site than either of those examined here and as such, the findings of Cardone and Perrone [75] are in line with the EAL results computed here. Similarly, Sousa and Monteiro [81] have analysed pre-1970 RC frames with masonry infills, in different Italian locations characterised by low to high seismicity, obtaining EAL ranging from 0.2% to 0.5% hence, again, in agreement with the results presented here. Ottonelli et al. [62] examined two case study URM buildings located in L'Aquila and reported EAL values between 0.55% and 0.68%, which again align reasonably well with the findings here considering the relative differences in seismicity. Lastly, Cornali et al. [82] examined existing PC frame buildings in Italy and reported EAL ratio between 0.51% and 0.71%, which again are in line with the results obtained here.

The breakdown in relative contribution to the EAL ratio arising from damage to the structural and non-structural elements listed in Table 3.3, in addition to losses from structural collapse or demolition due to excessive residual drift, are shown in Fig. 4.1(a). For each typology, the damage to non-structural elements is a major contributor to the EAL; accounting for around 70% and 90% of the loss in the RC and PC buildings, respectively. This is also observed for the URM building, although for the high seismicity case, there is a significant contribution from the structural collapse cases reflecting its increased vulnerability in this regard. These results are in line with the data collected by Taghavi and Miranda [83] regarding the relative contributions of non-structural elements and building contents to economic losses. Although school buildings were not explicitly considered by Taghavi and Miranda, the general trend is consistent. Examining these relative contributions further, Fig. 4.2 shows the relative contributions to the vulnerability curves shown in Fig. 4.1(b) as a function of return period. Again, the non-structural element damage tends to be the main contributor, especially at lower return periods. Although other sources of loss tend to grow with increasing return period (e.g. the structural damage and collapses in the PC building from 475 years onward), their overall contributions to the annualised losses shown in Fig. 4.1(a) remain relatively low. This is due to the lower weighting of these higher return periods when integrating over the seismic hazard curve. However, it is clear from Fig. 4.2 how losses from non-structural element damage tend to dominate at lower, more frequent return periods whereas the contributions from structural damage and collapse tend to grow with increasing return period.

4.2. Collapse assessment

While the previous section examined the EAL incurred from the costs associated with both repairing and rebuilding the schools during collapsing and non-collapsing cases, respectively, this section examines the collapse safety of each school building typology in further detail. For a school building, the nominal life was taken as 50 years, as per Table 2.2.I of the 2008 Italian National Code [22]. The usage class for a school was deemed Class III, meaning that the reference time-period was amplified by a factor of 1.5 to give a reference time-period of 75 years. Assuming a Poisson distribution, the collapse prevention limit state outlined in NTC 2008 was defined as the 5% probability of exceedance in the reference time-period and corresponds to a return period of 1463 years.

While the prescriptions of NTC 2008 were adopted to identify the acceptable collapse performance in Italy, the compliance criteria outlined in FEMA P695 [58] were adopted to quantitatively assess the collapse performance of the schools using more advanced techniques. The compliance criteria outlined in FEMA P695 were checked by verifying that the probability of collapse at the MCE event is $< 10\%$. The MCE event is typically defined as the 2475-year return period event in the US when using the FEMA P695 guidelines, but as NTC 2008 specifies 1463 years for the collapse prevention limit state in school buildings, this return period is adopted here. Fig. 4.3 illustrates this approach where the collapse fragility functions developed in Section 3.4 are used to determine the probability of collapse at the MCE intensity, IM_{MCE}, and assess whether this value was above or below the limit of 10%. The dispersion of the collapse fragility includes the record-to-record variability and modelling uncertainty only and did not incorporate the additional terms for test data quality and design requirements outlined in FEMA P695. This was because the test data

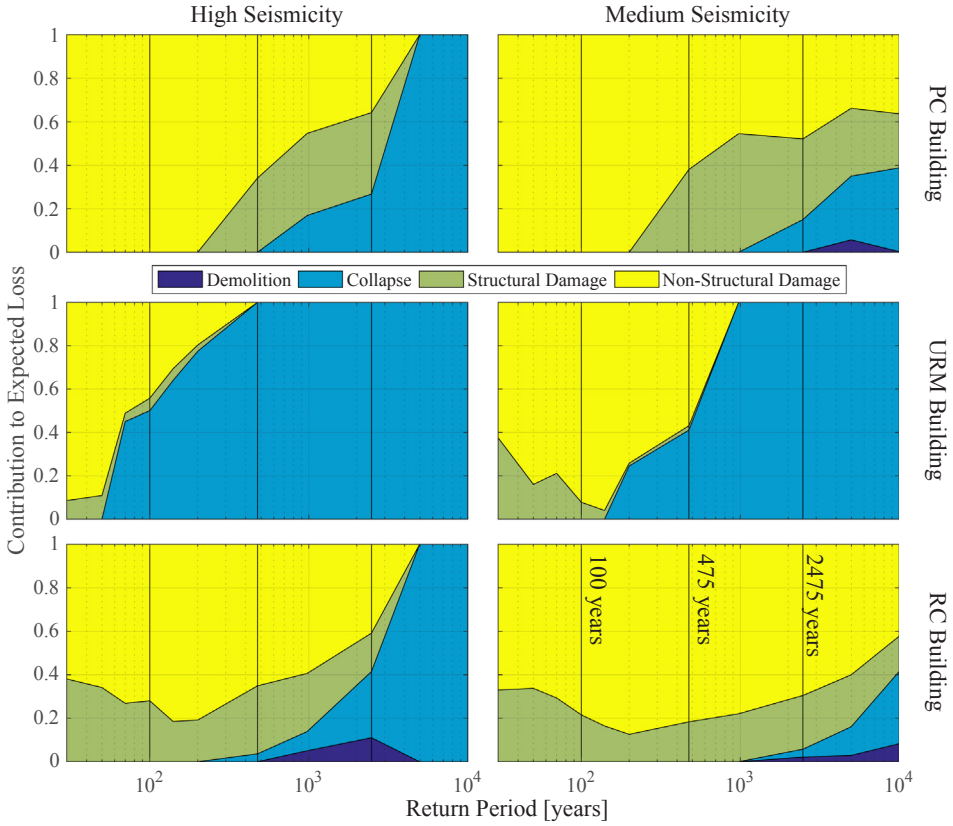

Fig. 4.2. Relative contribution to expected loss with respect to increasing return period for each building typology and site location considered. As a point of reference, the 100, 475 and 2475-year return periods have been annotated on each subplot.

amplification term was anticipated to be incorporated in the modelling uncertainty term outlined here and the design requirements were not deemed applicable in this case. To determine the corresponding intensity associated with the MCE event, the site hazard curves illustrated in Fig. 3.5 were utilised and the intensity associated with the intermediate 1463-year return period was established. Fig. 4.3 shows the resulting probabilities of collapse for each building typology at each of the site. While the procedure to assess collapse performance illustrated in Fig. 4.3 is somewhat specific to the FEMA P695 guidelines, another more robust measure of collapse performance is to integrate the collapse fragility over the entire hazard curve to obtain the mean annual frequency (MAF) of collapse. This is illustrated in Fig. 4.4 for each school building. Comparing the general trend between the two sites and the different school buildings in Fig. 4.3 and Fig. 4.4, it can be seen that the relative trends are similar. Regarding acceptable levels for the MAF of collapse of existing structures, Dolšek et al. [84] summarise some typical values from studies around the world and note that this limit typically lies in the range of 10^{-5} to 10^{-4}, which have been identified by the horizontal lines in Fig. 4.4 to evaluate the performance define in terms of MAF of collapse.

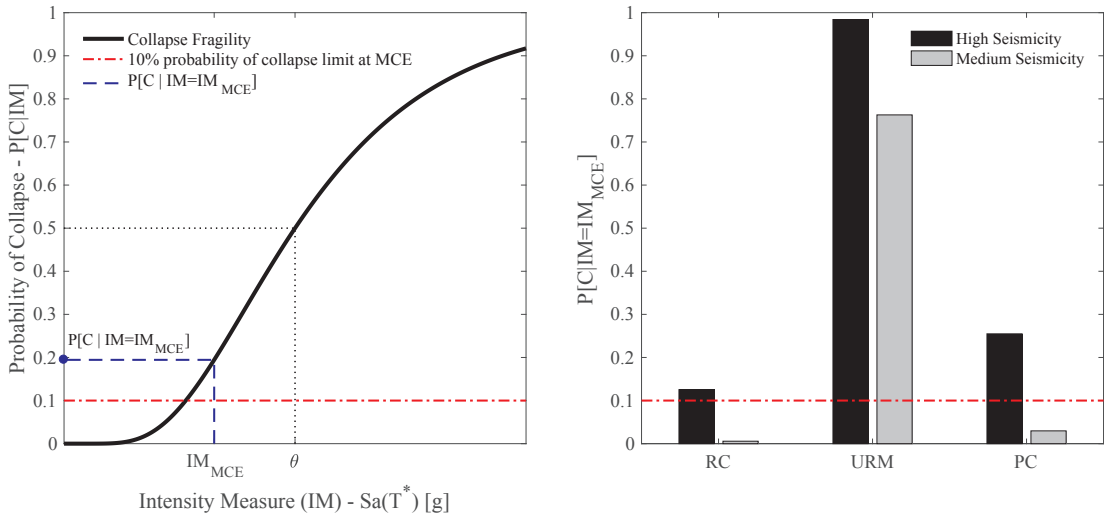

Fig. 4.3. Evaluation of the collapse criteria outlined in FEMA P695 for the different typologies, where the illustration on the left outlined the general approach and the values on the right report the probabilities of collapse at the MCE intensity for each building typology at the two site locations.

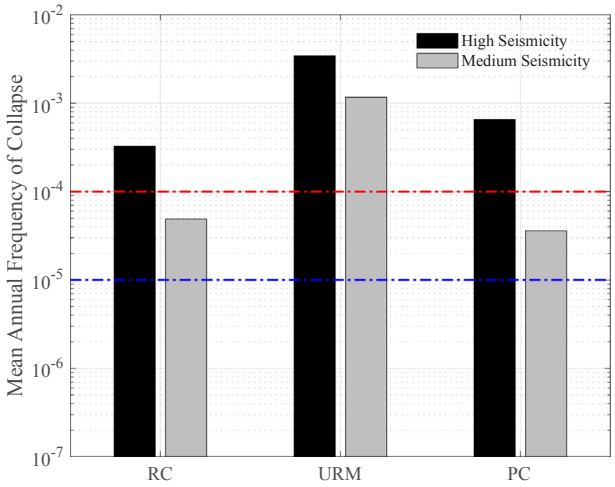

Fig. 4.4. Evaluation of collapse performance of school building characterised by the MAF of collapse. The range of acceptable limits corresponding to 10^{-4} (red line) and 10^{-5} (blue line) for the MAF of collapse described by Dolšek et al. [84] are also marked. (For interpretation of the references to colour in this figure legend, the reader is referred to the web version of this article.)

From observing the results, it is clear that the performance of the URM buildings is grossly unacceptable for both site locations. For instance, at the MCE event in Fig. 4.3, the URM school building is very likely to collapse for the two site locations considered in addition to the MAF of collapse shown in Fig. 4.4 far exceeding the acceptable levels of 10^{-5} or 10^{-4}. Furthermore, the RC and PC buildings fail the collapse criteria in Fig. 4.3 for the high seismicity location but pass in the case of the medium seismicity site. Fig. 4.4 shows the same relative trend for RC and PC buildings, with both of them exceeding the 10^{-4} limit at the high seismicity location, whereas the RC building just slightly exceeds this limit for the medium seismicity location. In terms of the collapse performance of the different school building typologies, the results shown above illustrate that in most cases the collapse performance is unacceptable and should be rectified through appropriate structural retrofitting since prevention of collapse safety is typically one of the fundamental requirements of seismic design. Such retrofitting should also be conducted in tandem with the EAL results presented in Section 4.1. Recent work by O'Reilly and Sullivan [85] has shown that structurally retrofitting a structure through strengthening and stiffening can be very effective in terms of improving the collapse performance but can be detrimental to EAL, i.e. retrofitting can actually result in a worsening of the EAL if appropriate care is not taken. This arises due to the fact that the benefits gained in limiting drift demand and reducing drift-sensitive losses through increased strength and stiffness, are counteracted by increased floor acceleration demands and increased losses in acceleration-sensitive non-structural elements, which can result in a net increase in EAL.

4.3. Comparison with Italian seismic risk classification guidelines

A document of particular relevance to the case study school buildings considered herein is the recent Italian seismic risk classification guidelines detailed in Decreto Ministeriale (D.M.) 58/2017 [20]. These guidelines aim to incorporate some of the more recent advancements in the field of seismic risk assessment into a procedure that is both straightforward to implement and integrates well with existing codes in Italy. The guidelines focus on two specific aspects regarding buildings; life safety and expected annual loss, and provide a classification system with which practitioners can assess the current status of buildings and demonstrate improvements in seismic performance via different retrofitting measures. The procedure is illustrated in Fig. 4.5 and shows how only a pushover analysis is required to identify the different limit states described in Italian national code [22] for each building typology. These four limit states are outlined qualitatively in NTC 2008 as follows:

- Stato Limite di Operatività – '*Operational*' (SLO): following the earthquake the building's structural and non-structural elements maintain their function and do not suffer any damage or significant interruption of their usage.
- Stato Limite di Danno – '*Damage Control*' (SLD): following the earthquake the buildings structural and non-structural elements suffer damage that does not put the occupants at risk and do not significantly compromise the overall capacity and stiffness of the structure to maintain the vertical and horizontal actions.
- Stato Limite di salvaguardia della Vita – '*Life Safety*' (SLV): following the earthquake the building suffers damage and failure to the non-structural elements and damage to the structural elements that results in a significant loss of lateral stiffness, but still maintains gravity load carrying capacity and a margin of safety against collapse.
- Stato Limite di prevenzione del Collasso – '*Collapse Prevention*' (SLC): following the earthquake the structure suffers heavy damage to both structural and non-structural elements; the structure maintains gravity load carrying capacity and has a slender margin of safety against collapse.

By identifying these four limit states for a case study building and converting it to an equivalent single degree-of-freedom (SDOF) system, as shown in Fig. 4.5(b) and (c), the intensity required to develop each of these is identified in Fig. 4.5(d). This intensity is defined in terms of the peak ground acceleration (PGA) of the code-defined acceleration spectrum. With this intensity, the mean annual frequency of exceedance (MAFE) is determined from a hazard model fitted to the available seismic hazard information since this information is typically available in discrete values of return period, as shown in Fig. 4.5(e). Once the MAFE for each of the limit states are established, these are then integrated with prescribed values of expected loss ratio for each limit state outlined in D.M. 58/2017 to compute the EAL as the area under the loss curve illustrated in Fig. 4.5(f). This approach is quite simple as it requires the analyst to conduct just a pushover analysis and eliminates the need for many of the steps involved in the PEER-PBEE loss estimation methodology discussed in Section 3. It is also analaogous to the more simplified assessment approaches recently outlined in the literature, such as Welch et al. [86] for example, with some more simplifying assumptions being made to better integrate it with existing code-based analysis methods that practicing engineers would be more familiar with. The end result of the guidelines is that an EAL is computed and classified within a latter-based system similar to that initially proposed by Calvi et al. [87]. In addition to the EAL-based score that classifies the seismic performance in terms of economic loss, another score is attributed based on the structural safety of the building. This is determined based on the ratio of the PGA required to develop the SLV limit state (PGA_{SLV} in Fig. 4.5(d)) to the PGA demand that structures are designed for at the same limit state. For example, a regular structure with a design life of 50 years would have a design return period of 475 years (10% probability of exceedance in 50 years), whereas school buildings would be designed for a return period of 712 years (10% probability of exceedance in 75 years). Using the demand to capacity ratio computed as function of the PGA at the SLV limit state, termed IS-V, another letter-based rank is attributed to the building and the overall ranking is determined as the more critical of the EAL-based and life safety-based ranks, which are listed in Table 4.2.

Following the simplified procedure outlined in D.M. 58/2017 and utilising the relevant analysis methods from NTC 2008, this simplified method was also applied to the three case study school buildings at both site locations to establish their seismic performance within these classification guidelines. Their performances were also compared with

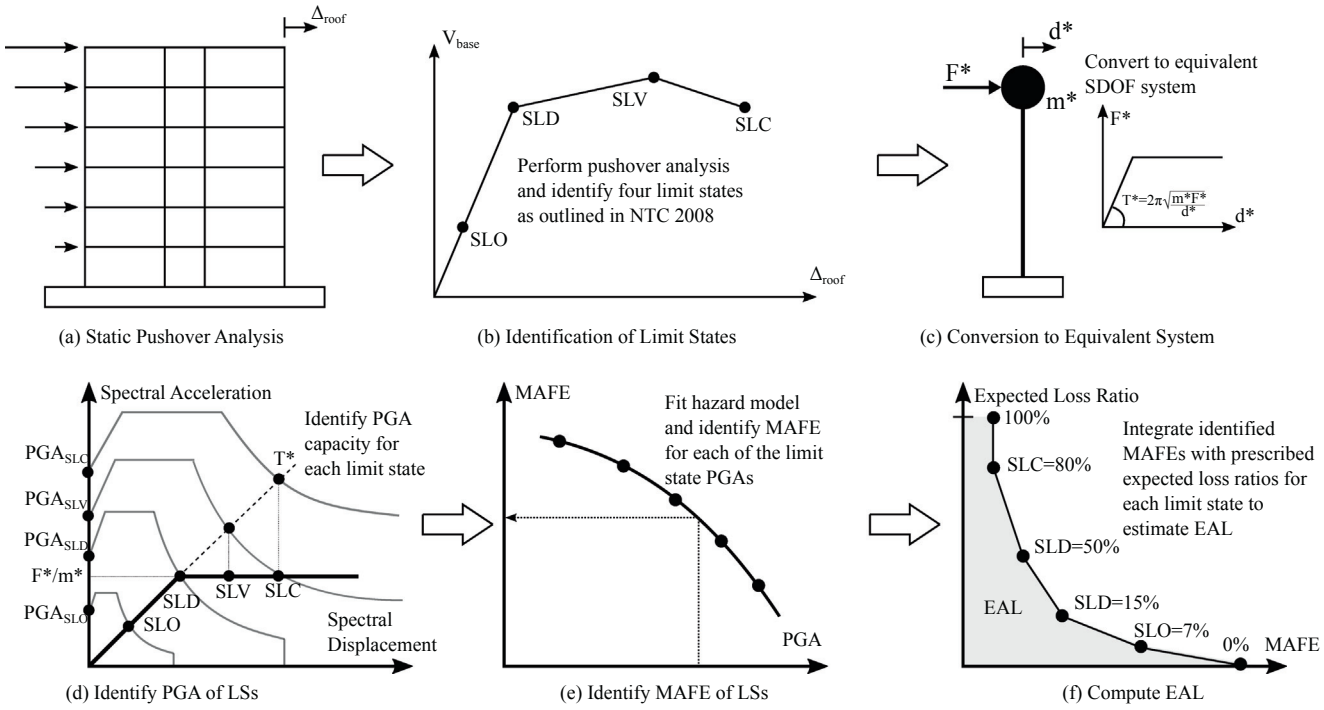

Fig. 4.5. Illustration of various steps within the Italian seismic risk classification scheme described in D.M. 58/2017 [20].

those computed following the rigorous approach outlined in Section 3. Each of the building models detailed in Section 3.2 was analysed using static pushover analyses, their limit states identified and their equivalent SDOF systems determined using the N2 method [88] prescribed in Appendix B of Eurocode 8: Part 1 [50], which is illustrated in Fig. 4.5(a)–(c). This was performed for the two principal directions of each school building and the PGA to exceed each limit state in either direction of the school building was determined, with the lesser of the two PGAs being adopted for final evaluation. While the guidelines anticipate the use of smoothed code spectra such as those illustrated in Fig. 4.5(d), the hazard model outlined in Section 3.3 was used here in order to maintain hazard consistency with the results of previous sections. The MAFE for each limit state were then determined, the EAL computed as per Fig. 4.5(f) and the final values are reported in Table 4.3. In addition, the life safety index (IS-V) was also computed as the ratio of the PGA_{SLV} determined in Fig. 4.5(d) and the PGA corresponding to a design return period of 712 years for school buildings. The scoring for both of these criteria was determined and the resulting overall seismic classification of the buildings is listed in Table 4.3.

By comparing the values presented in Table 4.3 first, it is clear that the life safety index is the governing criteria that determines the overall seismic classification in all but one case, with the URM buildings being observed to be particularly vulnerable when examining the IS-V indices. This is somewhat consistent with the previous findings presented in Sections 4.2, where the collapse performance was seen to be critical for the URM buildings. The guidelines note that for a new structure designed using NTC 2008, the IS-V score ought to be greater than or equal to unity. This again highlights the vulnerability of the existing school building stock in Italy, especially considering how the two site locations considered here do not represent locations of the highest seismicity in

Table 4.3
EAL and IS-V values computed using D.M. 58/2017 guidelines.

Site location	High seismicity			Medium seismicity		
Building typology	RC	URM	PC	RC	URM	PC
EAL	0.84%	1.01%	0.60%	0.60%	0.68%	0.48%
EAL Classification	A	B	A	A	A	A+
IS-V	0.60	0.50	0.90	0.79	0.67	1.20
IS-V Classification	C	C	A	B	B	A+
Overall Classification	**C**	**C**	**A**	**B**	**B**	**A+**

Table 4.2
Seismic performance classification ranking system as a function of both EAL and IS-V prescribed in D.M. 58/2017 [20].

EAL Classification Range	Life Safety Index Classification Range	Classification Ranking
EAL ≤ 0.5%	1.00 ≤ IS-V	A+
0.5% ≤ EAL < 1.0%	0.80 ≤ IS-V < 1.00	A
1.0% ≤ EAL < 1.5%	0.60 ≤ IS-V < 0.80	B
1.5% ≤ EAL < 2.5%	0.45 ≤ IS-V < 0.60	C
2.5% ≤ EAL < 3.5%	0.30 ≤ IS-V < 0.45	D
3.5% ≤ EAL < 4.5%	0.15 ≤ IS-V < 0.30	E
4.5% ≤ EAL < 7.0%	IS-V < 0.15	F
7.0% ≤ EAL		G

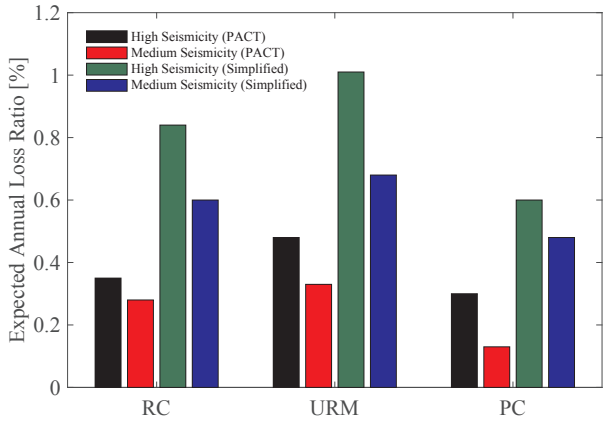

Fig. 4.6. Comparison of the EAL ratios from detailed analysis and those estimated from simplified analysis.

the Italian peninsula.

Comparing the EAL values reported in Table 4.3 with those computed using the rigorous approach in Section 4.1, some discrepancy can be seen in the results plotted in Fig. 4.6. The overall magnitude of the EAL values computed using the simplified method is much higher than those computed in Section 3. While the overall magnitude of the EAL computed using the two methods differs, the overall trend and relative differences between the different typologies and site locations remain the same. This suggests that, while the results obtained using the simplified methodology may not align closely with the values obtained from detailed analyses, the relative quantities remain similar and may still be used as a method with which to demonstrate a relative improvement in seismic performance. Nevertheless, even if conservative with respect to detailed analysis, the simplified seismic classification guidelines introduce more advanced means of quantifying seismic performance and offer a metric with which the overall seismic resilience of communities can be increased in addition to providing a motivation for stakeholders to upgrade the seismic performance of their buildings, as initially deliberated by Calvi et al. [87].

While the above comparison of the simplified assessment procedure indicates that the life safety performance of the school buildings at the different locations is not adequate; which aligns well with the detailed collapse performance results discussed in Section 4.2, the comparison of the absolute values of EAL between the detailed and simplified assessment methodologies differed significantly. These differences invariably arise from the simplifications required to integrate the procedure outlined in D.M. 58/2017 with existing codes of practice and make it more accessible to practising engineers. One of the main simplifications of the method to compute EAL in D.M. 58/2017 is the expected loss ratios for each limit state being fixed percentages of the replacement cost, regardless of building typology or occupancy. This aspect is further investigated here by comparing the expected loss ratio at each limit state for the case study buildings examined in Section 4.1 with the fixed expected loss ratios outlined in the guidelines. To do this, the exceedance of each limit state with respect to increasing intensity was identified and fragility functions were fitted in the same manner as for collapse outlined previously in Section 3.4. Using each of these limit state fragility functions and the vulnerability curves presented in Fig. 4.1(b), the expected loss ratio at each limit state from the detailed analysis was obtained by integrating these two, as illustrated in Fig. 4.7. This was necessary since the exceedance of a limit state is not a deterministic issue, but rather a probabilistic one that requires the exceedance distribution to be integrated with the expected loss ratio curve. Following this approach, the expected loss ratio at each limit state was computed for each school building and site location and is illustrated in Fig. 4.8. Also plotted are the fixed expected loss ratios specified in the guidelines and illustrated in Fig. 4.5(f). It is immediately apparent from Fig. 4.8 that the expected loss ratios at each limit state computed using the detailed analysis are lower than the fixed values specified in the D.M. 58/2017 guidelines. This discrepancy explains the difference in magnitude between the EAL values observed in Fig. 4.6; especially at the SLO and SLD limit states which are weighted much more heavily during the EAL integration. Furthermore, it was noted during the calculation of EAL using the simplified guidelines that the assumption that the initiation of damage begins at a fixed return period of 10 years (i.e. the MAFE of the point marked 0% in Fig. 4.5(f)) was very critical. Small changes in this threshold's return period definition significantly impacted the estimated EAL; for example, increasing this return period for the RC building at the high seismicity from 10 to 20 years reduced the EAL from 0.60% to 0.42%. Similarly, comparing the loss ratios at the different limit states outlined by Di Pasquale and Goretti [89] for URM buildings, for example, with those outlined in the recent guidelines, a notable discrepancy is also found. The values outlined in Di Pasquale and Goretti [89] tend to be lower than those prescribed in the guidelines for each limit state which further helps to explain the discrepancy reported in Fig. 4.6.

Lastly, another issue that may be further developed is regarding the building occupancy, where no distinction is made in the simplified guidelines between the different types of building occupancy for the building loss ratio at each limit state. Taghavi and Miranda [83] highlighted the importance of building occupancy type on the distribution of economic loss between the different elements of a building. More recently, Ramirez and Miranda [78] also proposed storey demand-to-loss functions for buildings and differentiating between building occupancy type. The occupancy type considered were school buildings so the general function provided in the guidelines may need to be refined for different building typologies.

5. Summary and conclusions

This paper has presented and discussed the seismic assessment of three existing school buildings located throughout Italy. These case study buildings, deemed representative of the Italian school building stock, were selected and chosen for further investigation within the scope of a national project to assess the seismic risk of Italian schools. These consisted of different structural typologies, namely reinforced concrete (RC) frames with masonry infill, unreinforced masonry (URM) and precast concrete (PC) frames. The PEER-PBEE seismic loss assessment framework was implemented in a systematic fashion to illustrate clearly its different steps. This involved first conducting in-situ surveys to help develop detailed numerical models capable of reproducing the structural behaviour over the full range of response up to structural collapse; in addition to documenting the non-structural elements and building contents needed for loss estimation. Using the modal analysis information provided by each numerical model, along with the seismic hazard disaggregation for two site locations in Italy of different seismicity level, ground motion records were selected for each building at a number of return periods, maintaining consistency with the seismic hazard characteristic of each site. The ground motion records for the two site locations were then used to analyse the response of the different building typologies and characterise their performance. Using the information collected through in-situ surveys and the building characterisation via numerical analyses, the different building typologies were assessed for both site locations in order to illustrate the overall performance of the school buildings for different levels of seismicity and to highlight the difference in performance between each construction typology found throughout Italy. This was discussed within the setting of existing Italian construction, where relevant information available from past earthquakes in Italy and communication with practitioners was incorporated into the assessment in order to make it as representative as possible. The expected annual loss (EAL) and collapse safety of the schools were then evaluated following the current state of the art PEER-PBEE methodology and the assessment

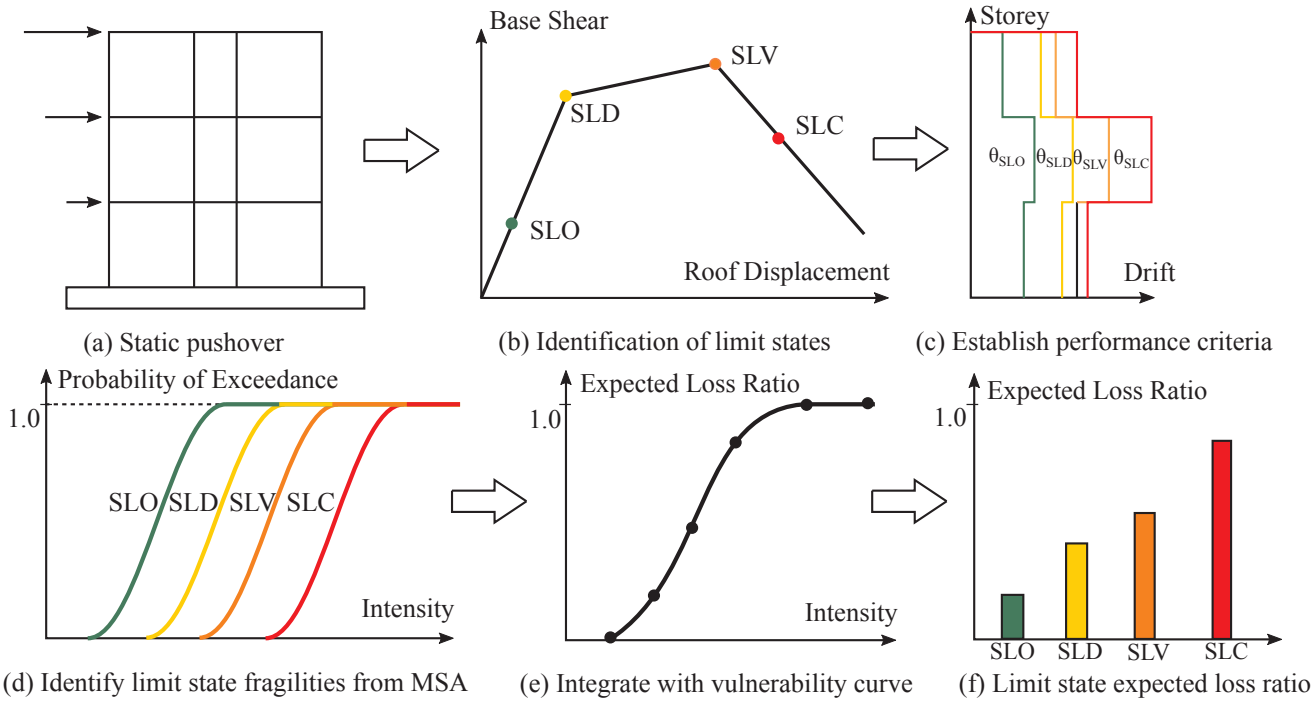

Fig. 4.7. Estimation of limit state expected loss ratio from MSA results.

guidelines recently proposed in Italy.

Based on the result of this study using three different building typologies and two different site locations, the following observations can be made:

- In general, this study has highlighted the seismic vulnerability of existing school buildings in Italy, both in terms of their vulnerability to losses through excessive structural and non-structural damage and in terms of their collapse capacity. This was observed for both site locations and each construction typology examined to highlight how measures ought to be taken to ensure the seismic safety of school buildings in Italy to avoid repeats of situations such as that of Molise in 2002.
- The EAL values computed following the rigorous PEER PBEE loss estimation methodology were below 1% for all typologies at the site locations considered. When compared to recent quantification studies on existing Italian buildings, these appear to be in line with typical values.
- In terms of construction typology, it was shown how the URM school building is the most vulnerable out of the three considered when assessing the expected losses with respect to increasing seismic intensity. This was reflected in the comparison of the EAL values for school buildings, where the URM building reported notably higher values compared to the other typologies. The RC and PC school buildings were also shown to be somewhat vulnerable when assessing the EAL values computed.
- Considering the relative contributions of structural and non-structural losses, structural collapse and residual drifts, it was shown how the damage to non-structural elements tends to dominate the expected annual loss, constituting between 70% and 90% of the total depending on the structural typology. This was further demonstrated to be a result of the large contribution of non-structural elements to the expected loss at more frequent return periods, whereas the contributions from structural damage and collapse grows with increasing intensity but at higher return periods.
- In terms of collapse capacity, the notably high collapse risk of the existing school building typologies was highlighted first using the FEMA P695 guidelines. This was evaluated in terms of the probability of collapse at the maximum credible event, which showed how the URM school building considered is at high risk of structural collapse for both site locations examined. This was also the case for the RC and PC buildings, where the collapse safety criteria were not satisfied for one of the site locations. Furthermore, computing the mean annual frequency of collapse via hazard curve integration shows that when compared to a typical range of acceptable limits from the literature, a similar trend was observed.

Comparing the findings of the extensive assessment approach outlined in Section 3 of this paper with the recent seismic performance classification guidelines, Decreto Ministeriale 58/2017, introduced in Italy in 2017 highlighted a number of issues. Firstly, in terms of assessing the life safety of existing buildings using simplified methods of analysis, the recent guidelines were consistent with the findings of the extensive analysis in that they highlighted the same buildings as being vulnerable to collapse. In terms of EAL, the recent guidelines earmarked the same structures as being vulnerable relative to each other. However, in terms of overall magnitude of the EAL computed compared to that calculated using the extensive assessment approach, a significant overestimation of the EAL was observed. Further examination of the expected loss ratio at each limit state from the detailed analysis with the values adopted by the guidelines highlighted the conservative nature of the guidelines, which was identified as the main source of discrepancy in the results. Furthermore, it was noted how more refined vulnerability functions for different building typologies and occupancy types may be needed for future improvement of the guidelines. Using any of the methodologies, refined or simplified, these loss assessment results will be fundamental in defining retrofitting schemes to improve the overall performance of the different school building typologies at different locations characterised by different seismicity levels. Specifically, cost-benefit analysis frameworks are envisaged to identify the optimum solutions in the Italian context as well as to allocate available resources.

Acknowledgements

The authors would like to acknowledge the funding provided by the Centro di Geomorfologia Integrata per l'Area del Mediterraneo

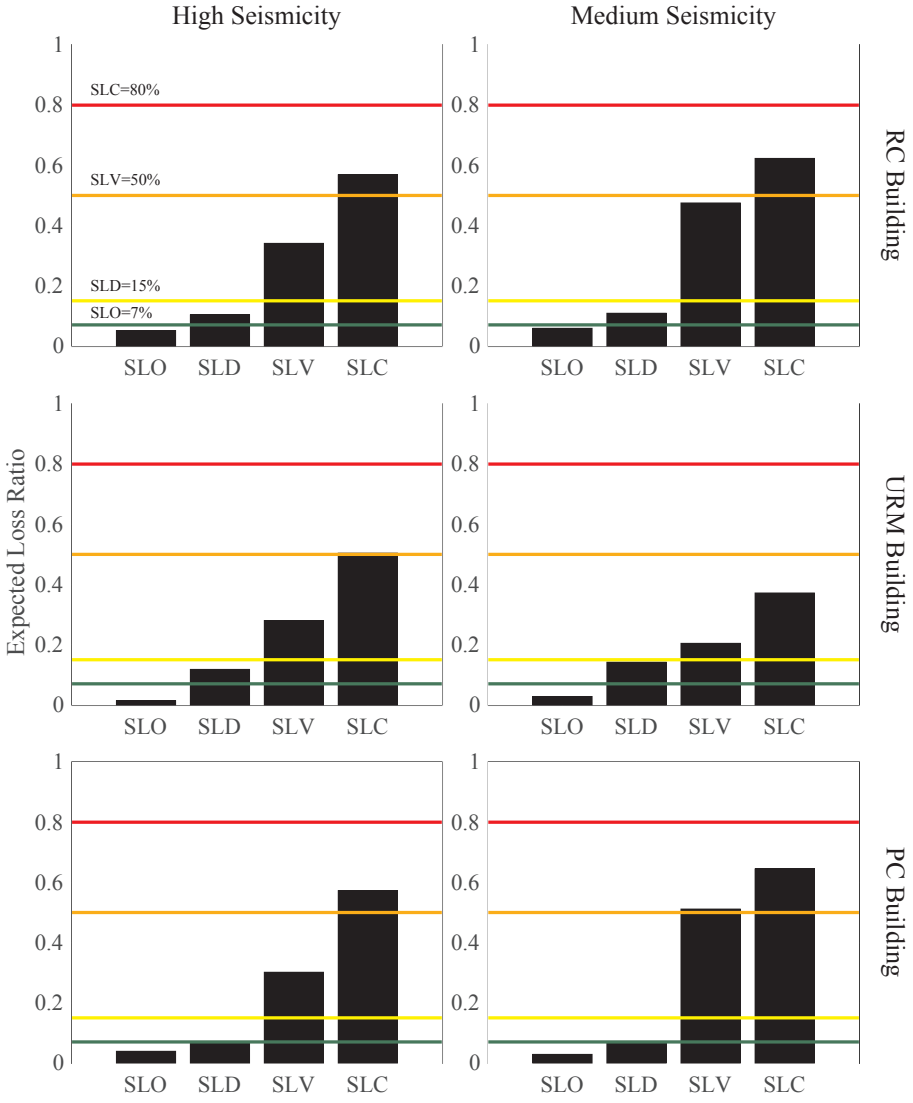

Fig. 4.8. Comparison of expected loss ratio computed from MSA and detailed loss estimation with simplified guidelines.

(CGIAM) and the European Centre for Training and Research in Earthquake Engineering (EUCENTRE). The authors wish to also acknowledge the help of Ing. Matteo Moratti from Studio Calvi S.r.l who provided information on various aspects discussed in Section 3.

References

[1] Borzi B, Ceresa P, Faravelli M, Fiorini E, Onida M. Definition of a prioritization procedure for structural retrofitting of Italian school buildings. COMPDYN 2011–3rd ECCOMAS Themat Conf Comput Methods Struct Dyn Earthq Eng, Corfu, Greece; 2011.
[2] Regio Decreto. Norme per l'esecuzione delle opere conglomerato cementizio semplice od armato – 2229/39. Rome, Italy; 1939.
[3] Vona M, Masi A. Resistenza sismica di telai in c.a. progettati con il R.D. 2229/39. XI Congr. Naz. "L'Ingegneria Sismica Ital., vol. 3274, Genova, Italia; 2004.
[4] O'Reilly GJ, Sullivan TJ, Filiatrault A, Moratti M, Calvi PM. Past Observations of Damage in Italian RC Structures. EUCENTRE Res Rep 2015.
[5] Augenti N, Parisi F. Learning from construction failures due to the 2009 L'Aquila, Italy, earthquake. J Perform Constr Facil 2010;24:536–55. http://dx.doi.org/10.1061/(ASCE)CF.1943-5509.0000122.
[6] Salvatore W, Caprilli S, Barberi V. Rapporto dei Danni Provocati dall'Evento Sismico del 6 Aprile sugli Edifici Scolastici del Centro Storico dell'Aquila. Pisa, Italy; 2009.
[7] Ricci P, De Luca F, Verderame GM. 6th April 2009 L'Aquila earthquake, Italy: reinforced concrete building performance. Bull Earthq Eng 2011;9:285–305. http://dx.doi.org/10.1007/s10518-010-9204-8.
[8] Verderame GM, Iervolino I, Ricci P. Report on the Damage on Buildings Following the Seismic Event of 6th of April 2009 Time 1:32 - L'Aquila M = 5.8; 2009.
[9] Kaplan H, Bilgin H, Yilmaz S, Binici H, Öztas A. Structural damages of L'Aquila (Italy) earthquake. Nat Hazards Earth Syst Sci 2010;10:499–507. http://dx.doi.org/10.5194/nhess-10-499-2010.
[10] Penna A, Morandi P, Rota M, Manzini CF, da Porto F, Magenes G. Performance of masonry buildings during the Emilia 2012 earthquake. Bull Earthq Eng 2014;12:2255–73. http://dx.doi.org/10.1007/s10518-013-9496-6.
[11] Cimellaro GP. Field Reconnaissance Following the April 6, 2009 L'Aquila Earthquake in Italy. Buffalo, USA; 2009.
[12] Beyer K, Dazio A. Quasi-Static Cyclic Tests on Masonry Spandrels. Earthq Spectra 2012;28:907–29. http://dx.doi.org/10.1193/1.4000063.
[13] Magliulo G, Ercolino M, Petrone C, Coppola O, Manfredi G. The Emilia earthquake: seismic performance of precast reinforced concrete buildings. Earthq Spectra 2014;30:891–912. http://dx.doi.org/10.1193/091012EQS285M.
[14] Miranda E, Mosqueda G, Retamales R, Pekcan G. Performance of nonstructural components during the 27 February 2010 Chile Earthquake. Earthq Spectra 2012;28. http://dx.doi.org/10.1193/1.4000032. S453-71.
[15] Braga F, Manfredi V, Masi A, Salvatori A, Vona M. Performance of non-structural elements in RC buildings during the L'Aquila, 2009 earthquake. Bull Earthq Eng 2010;9:307–24. http://dx.doi.org/10.1007/s10518-010-9205-7.
[16] Ercolino M, Petrone C, Coppola O, Magliulo G. Report sui danni registrati a San Felice sul Panaro (MO) in seguito agli eventi sismici del 20 e 29 maggio 2012. ReLUIS Rep 2012.
[17] Calvi PM, Moratti M, Filiatrault A. Studio della risposta di elementi non strutturali di edifici scolastici soggetti ad eventi sismici. Progett Sismica 2015;6.
[18] Cornell CA, Krawinkler H. Progress and challenges in seismic performance assessment. PEER Cent News 2000;3:1–2.
[19] Günay S, Mosalam KM. PEER performance-based earthquake engineering methodology, revisited. J Earthq Eng 2013;17:829–58. http://dx.doi.org/10.1080/13632469.2013.787377.
[20] Decreto Ministeriale. Linee Guida per la Classificazione del Rischio Sismico delle Costruzioni – 58/2017. Rome, Italy; 2017.
[21] EU Council. Council Directive 92/75/EEC of 22 September 1992 on the indication

by labelling and standard product information of the consumption of energy and other resources by household appliances. Brussels, Belgium; 1992.
[22] NTC. Norme Tecniche Per Le Costruzioni. Rome, Italy; 2008.
[23] FEMA P58-1. Seismic Performance Assessment of Buildings: Volume 1 - Methodology (P-58-1). vol. 1. Washington, DC; 2012.
[24] O'Reilly G, Monteiro R, Perrone D, Lanese I, Fox M, Pavese A, et al. System Identification and Structural Modelling of Italian School Buildings. In: Caicedo J, Pakzad S, editors. Dyn. Civ. Struct. Vol. 2, Conf. Proc. Soc. Exp. Mech. Ser., Springer International Publishing; 2017, p. 301–3. http://dx.doi.org/10.1007/978-3-319-54777-0_37.
[25] Lang D, Verbicaro M, Singh Y. Seismic vulnerability assessment of hospitals and schools based on questionnaire survey; 2009.
[26] Perrone D, Aiello MA, Pecce M, Rossi F. Rapid visual screening for seismic evaluation of RC hospital buildings. Structures 2015;3:57–70. http://dx.doi.org/10.1016/j.istruc.2015.03.002.
[27] FEMA E-74. Reducing the risks of nonstructural earthquake damage – a practical guide. Washington, DC, USA; 2012.
[28] Dipartimento Protezione Civile. Linee guida per la riduzione della vulnerabilità sismica di elementi non strutturali arredi e impianti; 2009.
[29] McKenna F, Scott MH, Fenves GL. Nonlinear finite-element analysis software architecture using object composition. J Comput Civ Eng 2010;24:95–107. http://dx.doi.org/10.1061/(ASCE)CP.1943-5487.0000002.
[30] O'Reilly GJ, Sullivan TJ. Modeling techniques for the seismic assessment of the existing Italian RC Frame Structures. J Earthq Eng 2017:1–35. http://dx.doi.org/10.1080/13632469.2017.1360224.
[31] Scott MH, Fenves GL. Plastic hinge integration methods for force-based beam-column elements. J Struct Eng 2006;132:244–52. http://dx.doi.org/10.1061/(ASCE)0733-9445(2006) 132:2(244).
[32] Zimos DK, Mergos PE, Kappos AJ. Shear hysteresis model for reinforced concrete elements including the post-peak range. In: COMPDYN 2015–5th ECCOMAS themat conf comput methods struct dyn earthq eng, Crete Island, Greece; 2015.
[33] Almeida JP, Correia AA, Pinho R. Elastic and inelastic analysis of frames with a force-based higher-order 3D beam element accounting for axial-flexural-shear-torsional interaction. In: M. P, V. P, N L, editors. Comput methods earthq eng, Springer, Cham; 2017. p. 109–28. http://dx.doi.org/10.1007/978-3-319-47798-5_5.
[34] Bacco V. Solaio in latero-cemento: Confronto con sistemi alternativi; 2009. http://www.solaioinlaterizio.it/user/ConfrontoAlternativi.pdf.
[35] O'Reilly GJ, Perrone D, Fox MJ, Lanese I, Monteiro R, Filiatrault A, Pavese A. System Identification and Seismic Assessment Modelling Implications for Italian School Buildings. J Perform Constr Facil 2019. (Accepted).
[36] Crisafulli FJ, Carr AJ, Park R. Analytical modelling of infilled frame structures – a general review. Bull New Zeal Soc Earthq Eng 2000;33:30–47.
[37] Hak S, Morandi P, Magenes G, Sullivan TJ. Damage control for clay masonry infills in the design of RC frame structures. J Earthq Eng 2012;16:1–35. http://dx.doi.org/10.1080/13632469.2012.670575.
[38] Lagomarsino S, Penna A, Galasco A, Cattari S. TREMURI program: an equivalent frame model for the nonlinear seismic analysis of masonry buildings. Eng Struct 2013;56:1787–99. http://dx.doi.org/10.1016/j.engstruct.2013.08.002.
[39] EN 1998-3:2005. Eurocode 8: Design of structures for earthquake resistance – Part 3: Assessment and retrofit of buildings. Brussels, Belgium; 2005.
[40] Carr AJ. RUAUMOKO – User Manual, Theory, and Appendices; 2007. http://www.civil.canterbury.ac.nz/ruaumoko/index.html.
[41] Sharpe RD. The seismic response of inelastic structures PhD Thesis University of Canterbury; 1974.
[42] Paulay T, Priestley MJN. Seismic design of reinforced concrete and masonry buildings. John Wiley & Sons, Ltd.; 1992.
[43] Otani S. Hysteresis models of reinforced concrete for earthquake response analysis. J Fac Eng 1981;36:125–59.
[44] Priestley MJN, Calvi GM, Kowalsky MJ. Displacement based seismic design of structures. Pavia, Italy: IUSS Press; 2007.
[45] Chopra AK, McKenna F. Modeling viscous damping in nonlinear response history analysis of buildings for earthquake excitation. Earthq Eng Struct Dyn 2016;45:193–211. http://dx.doi.org/10.1002/eqe.2622.
[46] Masi A, Vona M. Vulnerability assessment of gravity-load designed RC buildings: evaluation of seismic capacity through non-linear dynamic analyses. Eng Struct 2012;45:257–69. http://dx.doi.org/10.1016/j.engstruct.2012.06.043.
[47] Grant DN, Bommer JJ, Pinho R, Calvi GM, Goretti A, Meroni F. A prioritization scheme for seismic intervention in school buildings in Italy. Earthq Spectra 2012;23:291–314.
[48] Baker JW. Conditional mean spectrum: tool for ground-motion selection. J Struct Eng 2011;137:322–31. http://dx.doi.org/10.1061/(ASCE)ST.1943-541X.0000215.
[49] Jayaram N, Lin T, Baker JW. A computationally efficient ground-motion selection algorithm for matching a target response spectrum mean and variance. Earthq Spectra 2011;27:797–815. http://dx.doi.org/10.1193/1.3608002.
[50] EN 1998-1:2004. Eurocode 8: Design of structures for earthquake resistance – Part 1: General rules, Seismic Actions and Rules for Buildings. Brussels, Belgium; 2004.
[51] Lin T, Haselton CB, Baker JW. Conditional spectrum-based ground motion selection. Part I: Hazard consistency for risk-based assessments. Earthq Eng Struct Dyn 2013;42:1847–65. http://dx.doi.org/10.1002/eqe.2301.
[52] Ancheta TD, Darragh RB, Stewart JP, Seyhan E, Silva WJ, Chiou BSJ, et al. PEER NGA-West2 Database. PEER Rep 2013/03; 2013.
[53] Ambraseys NN, Simpson KA, Bommer JJ. Prediction of horizontal response spectra in Europe. Earthq Eng Struct Dyn 1996;25:371–400.
[54] Iervolino I, Chioccarelli E, Cito P. REASSESS V1.0: A computationally efficient software for probabilistic seismic hazard analysis. In: COMPDYN 2015–5th ECCOMAS themat conf comput methods struct dyn earthq Eng, Crete Island, Greece; 2015.
[55] Baker JW, Jayaram N. Correlation of spectral acceleration values from NGA ground motion models. Earthq Spectra 2008;24:299–317. http://dx.doi.org/10.1193/1.2857544.
[56] Bazzurro P, Cornell CA, Shome N, Carballo JE. Three proposals for characterizing MDOF nonlinear seismic response. J Struct Eng 1998;124:1281–9. http://dx.doi.org/10.1061/(ASCE)0733-9445(1998) 124:11(1281).
[57] Baker JW. Efficient analytical fragility function fitting using dynamic structural analysis. Earthq Spectra 2015;31:579–99. http://dx.doi.org/10.1193/021113EQS025M.
[58] FEMA P695. Quantification of building seismic performance factors. Washington, DC, USA; 2009.
[59] Vamvatsikos D, Cornell CA. Incremental dynamic analysis. Earthq Eng Struct Dyn 2002;31:491–514. http://dx.doi.org/10.1002/eqe.141.
[60] O'Reilly GJ, Sullivan TJ, Monteiro R. On the seismic assessment and retrofit of infilled RC frames structures. In: 16th Eur conf earthq Eng, Thessaloniki, Greece; 2018.
[61] Rossetto T, Elnashai A. Derivation of vulnerability functions for European-type RC structures based on observational data. Eng Struct 2003;25:1241–63. http://dx.doi.org/10.1016/S0141-0296(03)00060-9.
[62] Ottonelli D, Cattari S, Lagomarsino S. Assessment and retrofit of masonry structures. In: Sullivan TJ, Calvi GM, Monteiro R, editors. Towar simpl displac loss assess retrofit approaches, Pavia, Italy; 2016. p. 5–62.
[63] Morandi P, Albanesi L, Graziotti F, Li Piani T, Penna A, Magenes G. Development of a database on the in-plane experimental response of URM Piers 2017.
[64] Haselton CB, Deierlein GG. Assessing seismic collapse of modern reinforced concrete moment frame buildings. Blume Rep No 156; 2007.
[65] Priestley MJN, Seible F, Verma R, Xiao Y. Seismic shear strength of reinforced concrete columns. Rep SSRP-93/06; 1993.
[66] FEMA P58-3. Seismic Performance Assessment of Buildings Volume 3—Performance Assessment Calculation Tool (PACT) Version 2.9.65 (FEMA P-58-3.1). vol. 3. Washington, DC; 2012.
[67] Cardone D. Fragility curves and loss functions for RC structural components with smooth rebars. Earthquakes Struct 2016;10:1181–212. http://dx.doi.org/10.12989/eas.2016.10.5.1181.
[68] Cardone D, Perrone G. Developing fragility curves and loss functions for masonry infill walls. Earthquakes Struct 2015;9:257–79. http://dx.doi.org/10.12989/eas.2015.9.1.257.
[69] Sassun K, Sullivan TJ, Morandi P, Cardone D. Characterising the in-plane seismic performance of infill masonry. Bull New Zeal Soc Earthq Eng 2015;49.
[70] Regione Lombardia Infrastrutture e Mobilità. Prezziario delle opera pubbliche Regione Lombardia dei Tipografia del Genio Civile; 2011.
[71] Cornell CA, Jalayer F, Hamburger RO, Foutch DA. Probabilistic basis for 2000 SAC federal emergency management agency steel moment frame guidelines. J Struct Eng 2002;128:526–33. http://dx.doi.org/10.1061/(ASCE)0733-9445(2002) 128:4(526).
[72] O'Reilly GJ, Sullivan TJ. Quantification of modelling uncertainty in existing Italian RC frames. Earthq Eng Struct Dyn 2018;47:1054–74. http://dx.doi.org/10.1002/eqe.3005.
[73] O'Reilly GJ, Sullivan TJ. Modelling uncertainty in existing Italian RC frames. In: COMPDYN 2017–6th int conf comput methods struct dyn earthq eng, Rhodes Island, Greece; 2017. http://dx.doi.org/10.7712/120117.5445.16952.
[74] Decreto Legislativo 163/2006. Elenco regionale dei prezzi delle opere pubbliche della regione emilia-romagna – 163/2006; 2015.
[75] Cardone D, Perrone G. Damage and loss assessment of Pre-70 RC frame buildings with FEMA P-58. J Earthq Eng 2017;21:23–61. http://dx.doi.org/10.1080/13632469.2016.1149893.
[76] Dolce M, Manfredi G. Libro bianco sulla ricostruzione privata fuori dai centri storici nei comuni colpiti dal sisma dell'Abruzzo del 6 aprile 2009. Doppiavoce, Napoli, Italy; 2015.
[77] Elwood KJ, Marquis F, Kim JH. Post-earthquake assessment and repairability of RC buildings: lessons from Canterbury and emerging challenges. In: Proc tenth Pacific conf earthq eng, Sydney, Australia; 2015.
[78] Ramirez CM, Miranda E. Building specific loss estimation methods & tools for simplified performance based earthquake engineering. Blume Rep. No. 171; 2009.
[79] Villar-Vega M, Silva V. Assessment of earthquake damage considering the characteristics of past events in South America. Soil Dyn Earthq Eng 2017;99:86–96. http://dx.doi.org/10.1016/j.soildyn.2017.05.004.
[80] Kim JJ, Elwood KJ, Marquis F, Chang SE. Factors influencing post-earthquake decisions on buildings in Christchurch, New Zealand. Earthq Spectra 2017;33:623–40. http://dx.doi.org/10.1193/072516EQS120M.
[81] Sousa L, Monteiro R. Seismic retrofit options for non-structural building partition walls: impact on loss estimation and cost-benefit analysis. Eng Struct 2018;161:8–27. http://dx.doi.org/10.1016/j.engstruct.2018.01.028.
[82] Cornali F, Belleri A, Riva P. Assessment and Retrofit of Pre-Cast Concrete Buildings. In: Sullivan TJ, Calvi GM, Monteiro R, editors. Towar simpl displac loss assess. Retrofit Approaches, Pavia, Italy; 2016. p. 181–221.
[83] Taghavi S, Miranda E. Response assessment of nonstructural building elements. PEER Rep 2003/05; 2003.
[84] Dolšek M, Lazar Sinković N, Žižmond J. IM-based and EDP-based decision models for the verification of the seismic collapse safety of buildings. Earthq Eng Struct Dyn 2017;46:2665–82. http://dx.doi.org/10.1002/eqe.2923.
[85] O'Reilly GJ, Sullivan TJ. Probabilistic seismic assessment and retrofit considerations for Italian RC frame buildings. Bull Earthq Eng 2018;16:1447–85. http://dx.doi.org/10.1007/s10518-017-0257-9.

[86] Welch DP, Sullivan TJ, Calvi GM. Developing direct displacement-based procedures for simplified loss assessment in performance-based earthquake engineering. J Earthq Eng 2014;18:290–322. http://dx.doi.org/10.1080/13632469.2013.851046.
[87] Calvi GM, Sullivan TJ, Welch DP. A seismic performance classification framework to provide increased seismic resilience. In: 2nd Eur. Conf. Earthq. Eng. Seismol., Istanbul, Turkey; 2014.
[88] Fajfar P. A nonlinear analysis method for performance-based seismic design. Earthq Spectra 2000;16:573–92. http://dx.doi.org/10.1193/1.1586128.
[89] Di Pasquale G, Goretti A. Vulnerabilità funzionale ed economica degli edifici residenziali colpiti dai recenti eventi sismici italiani. In: Proc 10th natl conf "L'ingegneria Sismica Ital, Potenza-Matera, Italy; 2001.